REPORT DOCUMENTATION PAGE

Form Approved OMB NO. 0704-0188

1. REPORT DATE (DD-MM-YYYY)	2. REPORT TYPE	3. DATES COVERED (From - To)
18-03-2012	Final Report	5-Apr-2005 - 4-Nov-2011

4. TITLE AND SUBTITLE
Nanoscale Probing of Electrical Signals in Biological Systems

5a. CONTRACT NUMBER
W911NF-05-1-0177

5b. GRANT NUMBER

5c. PROGRAM ELEMENT NUMBER
611102

6. AUTHORS
Mark C. Hersam

5d. PROJECT NUMBER

5e. TASK NUMBER

5f. WORK UNIT NUMBER

7. PERFORMING ORGANIZATION NAMES AND ADDRESSES
Northwestern University Chicago Campus
Office of Sponsored Research
Northwestern University
Evanston, IL 60208 -1110

8. PERFORMING ORGANIZATION REPORT NUMBER

9. SPONSORING/MONITORING AGENCY NAME(S) AND ADDRESS(ES)
U.S. Army Research Office
P.O. Box 12211
Research Triangle Park, NC 27709-2211

10. SPONSOR/MONITOR'S ACRONYM(S)
ARO

11. SPONSOR/MONITOR'S REPORT NUMBER(S)
48138-CH-PCS.21

12. DISTRIBUTION AVAILIBILITY STATEMENT
Approved for Public Release; Distribution Unlimited

13. SUPPLEMENTARY NOTES
The views, opinions and/or findings contained in this report are those of the author(s) and should not contrued as an official Department of the Army position, policy or decision, unless so designated by other documentation.

14. ABSTRACT
An improved molecular-level description of trans-membrane ion currents has the potential to impact many areas of military and civilian importance such as disease diagnosis, drug development/screening, and technologies that interface between living cells and microelectronic circuitry. Ultimately, these developments would imply improvements in health and quality of life for individuals that have suffered from injuries or wounds that have compromised senses such as sight and hearing. Furthermore, technologies involving the human-machine interface

15. SUBJECT TERMS
conductive atomic force microscopy, scanning electrochemical microscopy, scanning ion conductance microscopy, nanoporous membranes, anodized aluminum oxide, atomic layer deposition, focused ion beam milling, nanopatterning, patch clamp,

16. SECURITY CLASSIFICATION OF:			17. LIMITATION OF ABSTRACT	15. NUMBER OF PAGES	19a. NAME OF RESPONSIBLE PERSON
a. REPORT	b. ABSTRACT	c. THIS PAGE			Mark Hersam
UU	UU	UU	UU		19b. TELEPHONE NUMBER: 847-491-2696

Report Title

Nanoscale Probing of Electrical Signals in Biological Systems

ABSTRACT

An improved molecular-level description of trans-membrane ion currents has the potential to impact many areas of military and civilian importance such as disease diagnosis, drug development/screening, and technologies that interface between living cells and microelectronic circuitry. Ultimately, these developments would imply improvements in health and quality of life for individuals that have suffered from injuries or wounds that have compromised senses such as sight and hearing. Furthermore, technologies involving the human-machine interface and disease diagnosis/treatment are likely to be positively impacted. This AROYIP/PECASE, entitled "Nanoscale Probing of Electrical Signals in Biological Systems," is developing conductive atomic force microscopy (AFM) techniques, such as scanning electrochemical microscopy (SECM) and scanning ion conductance microscopy (SICM), with the potential to improve the spatial resolution of trans-membrane ion channel measurements by at least an order of magnitude over the current state-of-the art. In addition, nanostructured biocompatible neural stimulation electrodes are being fabricated and characterized. Beyond trans-membrane ion channels, advanced SECM and SICM methods have also been applied to other materials systems including electrochemically active electrodes, nanocomposites, graphene, and photovoltaics.

Enter List of papers submitted or published that acknowledge ARO support from the start of the project to the date of this printing. List the papers, including journal references, in the following categories:

(a) Papers published in peer-reviewed journals (N/A for none)

Received	Paper	
2012/03/18 2:	20	Albert L. Lipson, Ryan S. Ginder, Mark C. Hersam. Nanoscale In Situ Characterization of Li-ion Battery Electrochemistry Via Scanning Ion Conductance Microscopy, Advanced Materials, (12 2011): 0. doi: 10.1002/adma.201103094
2012/03/18 2:	19	Benjamin J. Leever, Ian P. Murray, Michael F. Durstock, Tobin J. Marks, Mark C. Hersam. Influence of Indium Tin Oxide Surface Treatment on Spatially Localized Photocurrent Variations in Bulk Heterojunction Organic Photovoltaic Devices, The Journal of Physical Chemistry C, (11 2011): 0. doi: 10.1021/jp209570h
2012/03/18 2:	18	M. C. Hersam. Monitoring and Analyzing Nonlinear Dynamics in Atomic Force Microscopy, Small, (10 2006): 0. doi: 10.1002/smll.200600272
2012/03/18 2:	17	M. J. Schmitz, M. C. Hersam, C. R. Kinser. Kinetics and Mechanism of Atomic Force Microscope Local Oxidation on Hydrogen-Passivated Silicon in Inert Organic Solvents, Advanced Materials, (06 2006): 0. doi: 10.1002/adma.200501231
2011/08/19 1:	16	Christopher Chen, Jun Liu, Tobin J. Marks, Mark C. Hersam, Norma E. Sosa. Large-Scale, Non-Subtractive Patterning of Transparent Conducting Oxides by Ion Bombardment, Applied Physics Letters, (07 2011): 22110. doi:
2011/08/19 1:	14	Michael D. Irwin, Jonathan D. Servaites, D. Bruce Buchholz, Benjamin J. Leever, Jun Liu, Jonathan D. Emery, Ming Zhang, Jung-Hwan Song, Michael F. Durstock, Arthur J. Freeman, Michael J. Bedzyk, Mark C. Hersam, Robert P. H. Chang, Mark A. Ratner, Tobin J. Marks. Structural and Electrical Functionality of NiO Interfacial Films in Bulk Heterojunction Organic Solar Cells, Chemistry of Materials, (04 2011): 2218. doi: 10.1021/cm200229e
2011/08/19 1:	15	Qing Hua Wang, Justice M. P. Alaboson, Joshua A. Kellar, Joohee Park, Jeffrey W. Elam, Michael J. Pellin, Mark C. Hersam. Conductive Atomic Force Microscope Nanopatterning of Epitaxial Graphene on SiC(0001) in Ambient Conditions, Advanced Materials, (05 2011): 2181. doi: 10.1002/adma.201100367
2011/01/13 0	13	D. J. Comstock, S. T. Christensen, J. W. Elam, M. J. Pellin, and M. C. Hersam. Synthesis of nanoporous activated iridium oxide films by anodized aluminum oxide templated atomic layer deposition, Electrochemistry Communications, (08 2010): . doi:
2011/01/13 0	12	D. J. Comstock, S. T. Christensen, J. W. Elam, M. J. Pellin, and M. C. Hersam. Tuning the composition and nanostructure of Pt/Ir films via anodized aluminum oxide templated atomic layer deposition, Advanced Functional Materials, (08 2010): . doi:
2010/09/02 1(	11	Norma E. Sosa, Christopher Chen, Jun Liu, Sujing Xie, Tobin J. Marks, Mark C. Hersam. Nanoscale Structure, Composition, and Charge Transport Analysis of Transparent Conducting Oxide Nanowires Written by Focused Ion Beam Implantation, Journal of the American Chemical Society, (08 2010): . doi:
2010/09/02 1(	10	David J. Comstock, Jeffrey W. Elam, Michael J. Pellin, Mark C. Hersam. Integrated ultramicroelectrode-nanopipette probe for concurrent scanning electrochemical microscopy and scanning ion conductance microscopy, Analytical Chemistry, (08 2010): . doi:
2010/09/02 1(	9	Michael D. Irwin, Jun Liu, Benjamin J. Leever, Jonathan D. Servaites, Mark C. Hersam, Michael F. Durstock, and Tobin J. Marks. Consequences of Anode Interfacial Layer Deletion. HCl-Treated ITO in P3HT:PCBM-Based Bulk-Heterojunction Organic Photovoltaic Devices, Langmuir, (03 2010): . doi:
2009/12/30 1:	6	A. L. Lipson, D. J. Comstock, M. C. Hersam. Nanoporous templates and membranes formed by nanosphere lithography and aluminum anodization, Small, (12 2009): . doi:
2009/03/16 0(	5	B. J. Leever, M. F. Durstock, M. D. Irwin, A. W. Hains, T. J. Marks, L. S. C. Pingree, and M. C. Hersam. Spatially resolved photocurrent mapping of operating organic photovoltaic devices using atomic force photovoltaic microscopy, Applied Physics Letters, (01 2008): . doi:
2009/03/16 0(	4	J. W. Elam, A. V. Zinovev, M. J. Pellin, D. J. Comstock, and M. C. Hersam. Nucleation and growth of noble metals on oxide surfaces using atomic layer deposition, ECS Transactions, (03 2007): . doi:
2009/03/16 0(	3	L. S. C. Pingree, M. J. Schmitz, D. E. Kramer, and M. C. Hersam. Laser assisted field induced oxide nanopatterning of hydrogen passivated silicon surfaces, Applied Physics Letters, (08 2007): . doi:

2009/03/16 0(	2	M. J. Schmitz, C. R. Kinser, N. E. Cortes, and M. C. Hersam. Ambient atomic force microscope nanoscale oxidation of hydrogen-passivated silicon with conductive diamond coated probes, Wiley InterScience, (03 2007): . doi:
2009/03/16 0(	1	N. E. Sosa, J. Liu, C. Chen, T. J. Marks, and M. C. Hersam. Nanoscale writing of transparent conducting oxide features with a focused ion beam, Advanced Materials, (02 2009): . doi:

TOTAL: **18**

Number of Papers published in peer-reviewed journals:

(b) Papers published in non-peer-reviewed journals (N/A for none)

Received	Paper

TOTAL:

Number of Papers published in non peer-reviewed journals:

(c) Presentations

(*indicated invited talk)

*[1] M. C. Hersam, “Functional inks based on monodisperse carbon nanomaterials,” presented orally by M. C. Hersam at the FACSS Society for Applied Spectroscopy National Meeting, Reno, Nevada (10/4/11).

*[2] M. C. Hersam, “Nanotechnology long-term impacts and research directions,” presented orally by M. C. Hersam at the FBI Industrial Security Advisory Council Meeting, Chicago, Illinois (9/22/11).

*[3] M. C. Hersam, “Chemically refined carbon nanoelectronic materials,” presented orally by M. C. Hersam at the AVS Prairie Chapter Symposium, Evanston, Illinois (9/1/11).

*[4] M. C. Hersam, “Molecular-scale tailoring of graphene surface chemistry via organic functionalization,” presented orally by M. C. Hersam at the NT11 Graphene Technology Satellite Workshop, Cambridge, United Kingdom (7/15/11).

*[5] M. C. Hersam, “Probing photon-matter and electron-matter interactions at the molecular scale,” presented orally by M. C. Hersam at the 7th Annual Meeting on Condensed Phase and Interfacial Molecular Science, Baltimore, Maryland (6/13/11).

*[6] M. C. Hersam, “Molecular-scale tailoring of graphene surface chemistry via organic functionalization,” presented orally by M. C. Hersam at the Brookhaven National Laboratory Epitaxial Graphene Workshop, Upton, New York (5/25/11).

*[7] M. C. Hersam, “Molecular-scale tailoring of graphene surface chemistry via organic functionalization,” presented orally by M. C. Hersam at the 219th Electrochemical Society Meeting, Montreal, Canada (5/3/11).

*[8] M. C. Hersam, “Fundamentals and applications of monodisperse carbon nanomaterials,” presented orally by M. C. Hersam at the 219th Electrochemical Society Meeting, Montreal, Canada (5/2/11).

*[9] M. C. Hersam, “Chemical functionalization of graphene,” presented orally by M. C. Hersam at the Cornell University Baker Symposium, Ithaca, New York (4/30/11).

*[10] M. C. Hersam, “Molecular-scale tailoring of graphene surface chemistry via organic functionalization,” presented orally by M. C. Hersam at the 2011 Materials Research Society Spring Meeting, San Francisco, California (4/27/11).

[11] A. L. Lipson and M. C. Hersam, “Nanoscale in situ characterization of Li-ion battery electrochemistry via scanning ion conductance microscopy,” presented orally by A. L. Lipson at the 2011 Materials Research Society Spring Meeting, San Francisco, California (4/27/11).

*[12] M. C. Hersam, “Fundamentals and applications of monodisperse carbon nanomaterials,” presented orally by M. C. Hersam at the 2011 Materials Research Society Spring Meeting, San Francisco, California (4/26/11).

*[13] M. C. Hersam, “Chemical methods for enhancing the performance of carbon nanoelectronic materials,” presented orally by M. C. Hersam at the Villa Conference on Interactions among Nanostructures, Las Vegas, Nevada (4/21/11).

*[14] M. C. Hersam, “Chemically functionalized carbon nanomaterials,” presented orally by M. C. Hersam at the California NanoSystems Institute Seminar Series, Los Angeles, California (4/5/11).

*[15] M. C. Hersam, “Characterization and opportunities for organically functionalized carbon nanomaterials,” presented orally by M. C. Hersam at the US-India-Israel Workshop on Nanoscale Phenomena in Soft and Hybrid Matter, Evanston, Illinois (3/23/11).

*[16] M. C. Hersam, “Fundamentals and applications of monodisperse carbon-based nanomaterials,” presented orally by M. C. Hersam at the 2011 American Physical Society March Meeting, Dallas, Texas (3/21/11).

*[17] M. C. Hersam, “Fundamentals and applications of monodisperse carbon nanomaterials,” presented orally by M. C. Hersam at the 25th International Winterschool on Electronic Properties of Novel Materials, Kirchberg, Austria (2/28/11).

*[18] M. C. Hersam, “Fundamentals and applications of monodisperse carbon nanomaterials,” presented orally by M. C. Hersam at the Rutgers University Institute for Advanced Materials, Devices and Nanotechnology Seminar Series, Piscataway, New Jersey (2/9/11).

*[19] M. C. Hersam, “Fundamentals and applications of monodisperse carbon nanomaterials,” presented orally by M. C. Hersam at the Nanotechnology for Clean Energy IGERT Seminar Series, Princeton, New Jersey (2/8/11).

*[20] M. C. Hersam, “Fundamentals and applications of monodisperse carbon nanomaterials,” presented orally by M. C. Hersam at the Indiana University Chemistry Department Materials Seminar Series, Bloomington, Indiana (1/25/11).

*[21] M. C. Hersam, “Fundamentals and applications of monodisperse carbon-based nanomaterials,” presented orally by M. C. Hersam at the University of Illinois Nanoelectronics and Photonics Seminar Series, Urbana, Illinois (1/24/11).

*[22] M. C. Hersam, “Chemically enhanced carbon-based nanoelectronic materials and devices,” presented orally by M. C. Hersam at the International Chemical Congress of Pacific Basin Societies, Honolulu, Hawaii (12/18/10).

*[23] M. C. Hersam, “Fundamentals and applications of monodisperse carbon-based nanomaterials,” presented orally by M. C. Hersam at the International Conference on NanoScience and NanoTechnology, Oryonghall, GIST, Korea (11/8/10).

*[24] M. C. Hersam, “Fundamentals and applications of monodisperse carbon-based nanomaterials,” presented orally by M. C. Hersam at the Mexican Physical Society Annual Meeting, Boca del Río, Veracruz, Mexico (10/28/10).

*[25] M. C. Hersam, “Chemically tailoring graphene via organic self-assembled monolayers,” presented orally by M. C. Hersam at the 57th AVS International Symposium, Albuquerque, New Mexico (10/19/10).

*[26] M. C. Hersam, “Blurring the boundaries: Opportunities for medicine at the interface between the physical and life sciences,” presented orally by M. C. Hersam at the Alumnae Continuing Education Forum, Evanston, Illinois (10/14/10).

*[27] M. C. Hersam, “Chemically enhanced carbon-based nanoelectronic materials and devices,” presented orally by M. C. Hersam at the NSF-MEXT US-Japan Young Scientists Symposium, Evanston, Illinois (10/6/10).

*[28] M. C. Hersam, “Fundamentals and applications of monodisperse carbon-based nanomaterials,” presented orally by M. C. Hersam at the 4th NIST Carbon Nanotube Workshop, Gaithersburg, Maryland (9/23/10).

*[29] M. C. Hersam, “Molecular-scale tailoring of graphene surface chemistry via organic functionalization,” presented orally by M. C. Hersam at the Workshop on Carbon Based Electronics, Albany, New York (9/22/10).

*[30] M. C. Hersam, “Chemically enhanced carbon-based nanomaterials and devices,” presented orally by M. C. Hersam at the Purdue University Department of Chemistry Colloquium, West Lafayette, Indiana (9/9/10).

*[31] M. C. Hersam, “Ultra-high vacuum processing and characterization of chemically functionalized graphene,” presented orally by M. C. Hersam at the 18th International Vacuum Congress and International Conference on Nanoscience and Technology, Beijing, China (8/24/10).

[32] M. C. Hersam, “Enhancing carbon-based nanomaterials and devices via chemical processing,” presented orally by M. C. Hersam at the Center for Integrated Nanotechnologies Users Conference, Albuquerque, New Mexico (8/11/10).

*[33] M. C. Hersam, “Chemically enhanced carbon-based nanoelectronic materials and devices,” presented orally by M. C. Hersam at the Nanoelectronics Research Initiative e-Workshop Series, Evanston, Illinois (5/25/10).

*[34] M. C. Hersam, “Preparation, characterization, and application of monodisperse carbon-based nanomaterials,” presented orally by M. C. Hersam at the 7th Annual Conference on the Foundations of Nanoscience, Snowbird, Utah (4/29/10).

*[35] M. C. Hersam, “Ultra-high vacuum processing and characterization of chemically functionalized graphene,” presented orally by M. C. Hersam at the 217th Electrochemical Society Meeting, Vancouver, Canada (4/27/10).

*[36] M. C. Hersam, “Preparation, characterization, and application of monodisperse carbon-based nanomaterials,” presented orally by M. C. Hersam at the 217th Electrochemical Society Meeting, Vancouver, Canada (4/26/10).

*[37] M. C. Hersam, “Preparation, characterization, and application of monodisperse carbon-based nanomaterials,” presented orally by M.

C. Hersam at the 2010 ChemOnTubes Conference, Arcachon, France (4/12/10).

*[38] N. L. Yoder and M. C. Hersam, "Preparation, characterization, and application of monodisperse carbon-based nanomaterials," presented orally by N. L. Yoder at the Onera Workshop on Optoelectronic Applications of Carbon Nanotubes, Chatillon, France (4/8/10).

*[39] M. C. Hersam, "Chemically enhanced carbon-based nanoelectronic materials and devices," presented orally by M. C. Hersam at the 2010 Materials Research Society Spring Meeting, San Francisco, California (4/7/10).

*[40] M. C. Hersam, "Enhancing carbon-based nanomaterials and devices via chemical processing," presented orally by M. C. Hersam at the Case Western Reserve University Department of Chemical Engineering Seminar Series, Cleveland, Ohio (2/18/10).

*[41] M. C. Hersam, "Chemically tailored carbon-based nanoelectronic materials and devices," presented orally by M. C. Hersam at the University of Chicago Department of Chemistry Colloquium, Chicago, Illinois (1/11/10).

*[42] M. C. Hersam, "Chemically tailored carbon-based nanoelectronic materials and devices," presented orally by M. C. Hersam at the 2009 Materials Research Society Fall Meeting, Boston, Massachusetts (12/1/09).

*[43] M. C. Hersam, "Chemically tailored carbon-based nanoelectronic materials and devices," presented orally by M. C. Hersam at the University of Connecticut Polymer Program Seminar Series, Storrs, Connecticut (11/20/09).

*[44] M. C. Hersam, "Chemically tailored carbon-based nanoelectronic materials and devices," presented orally by M. C. Hersam at the Princeton University Department of Chemistry Seminar Series, Princeton, New Jersey (8/11/09).

*[45] M. C. Hersam, "Optical and electronic properties of monodisperse carbon nanotube materials and devices," presented orally by M. C. Hersam at the 2009 SPIE Optics and Photonics Conference, San Diego, California (8/5/09).

*[46] M. C. Hersam, "Chemically tailored carbon-based nanoelectronic materials and devices," presented orally by M. C. Hersam at the 9th IEEE International Conference on Nanotechnology, Genoa, Italy (7/28/09).

*[47] M. C. Hersam, "Preparation and characterization of monodisperse carbon nanotube materials and devices," presented orally by M. C. Hersam at the Chinese Academy of Sciences Zhong Guan Cun Forum, Beijing, China (6/25/09).

*[48] M. C. Hersam, "Preparation and characterization of monodisperse carbon nanotube materials and devices," presented orally by M. C. Hersam at the 10th International Conference on the Science and Application of Nanotubes, Beijing, China (6/23/09).

*[49] M. C. Hersam, "Processing and properties of monodisperse single-walled and double-walled carbon nanotubes," presented orally by M. C. Hersam at the 215th Electrochemical Society Meeting, San Francisco, California (5/26/09).

*[50] M. C. Hersam, "Functionalized carbon nanotubes: Processing, characterization, and applications," presented orally by M. C. Hersam at the Northwestern University Division of Rheumatology Seminar Series, Chicago, Illinois (5/21/09).

*[51] M. C. Hersam, "Processing and properties of monodisperse carbon-based nanoelectronic materials," presented orally by M. C. Hersam at the 38th American Chemical Society Great Lakes Regional Meeting, Lincolnshire, Illinois (5/14/09).

*[52] M. C. Hersam, "Self-assembled monolayers on graphene surfaces: Prospects for graphene-based molecular electronics," presented orally by M. C. Hersam at the 2009 Materials Research Society Spring Meeting, San Francisco, California (4/13/09).

*[53] M. C. Hersam, "Introduction to nanometer scale science and technology," presented orally by M. C. Hersam at the Nanoscale Informal Science Education Network NanoDays Event, Evanston, Illinois (4/4/09).

*[54] M. C. Hersam, "Chemically tailored carbon-based nanoelectronic materials," presented orally by M. C. Hersam at the 237th American Chemical Society National Meeting, Salt Lake City, Utah (3/23/09).

*[55] M. C. Hersam, "Nanomaterials for electronics, sensing, and alternative energy," presented orally by M. C. Hersam at the Illinois Biotechnology Industry Organization Exposition, Chicago, Illinois (3/18/09).

*[56] M. C. Hersam, “Monodisperse colloidal suspensions of surfactant-encapsulated carbon nanotubes,” presented orally by M. C. Hersam at the Colloid and Surfactant Science Basic Research Workshop, Napa, California (3/12/09).

*[57] M. C. Hersam, “Preparation and characterization of monodisperse carbon nanotube materials and devices,” presented orally by M. C. Hersam at the Berkeley Sensor and Actuator Center Industrial Advisory Board Meeting, Berkeley, California (3/11/09).

*[58] M. C. Hersam, “Preparation, characterization, and application of monodisperse single-walled and double-walled carbon nanotubes,” presented orally by M. C. Hersam at the 23rd International Winterschool on Electronic Properties of Novel Materials, Kirchberg, Austria (3/8/09).

*[59] M. C. Hersam, “Preparation and characterization of monodisperse carbon nanotube materials and devices,” presented orally by M. C. Hersam at the Hillsdale College Department of Chemistry Seminar Series, Hillsdale, Michigan (2/24/09).

*[60] M. C. Hersam, “Preparation and characterization of monodisperse carbon nanotube materials and devices,” presented orally by M. C. Hersam at the Duke University Bioengineering Seminar Series, Durham, North Carolina (2/12/09).

*[61] M. C. Hersam, “Preparation and characterization of monodisperse carbon nanotube materials and devices,” presented orally by M. C. Hersam at the University of California at Irvine Chemical Engineering and Materials Science Colloquium, Irvine, California (2/6/09).

*[62] M. C. Hersam, “Preparation and characterization of monodisperse carbon nanotube materials and devices,” presented orally by M. C. Hersam at the University of Pennsylvania Materials Science and Engineering Colloquium, Philadelphia, Pennsylvania (1/22/09).

*[63] M. C. Hersam, “Introduction to nanometer scale science and technology,” presented orally by M. C. Hersam at Schiff Hardin LLP, Chicago, Illinois (1/15/09).

*[64] M. C. Hersam, “Introduction to nanometer scale science and technology,” presented orally by M. C. Hersam at the Nanotechnology Town Hall Meeting, Evanston, Illinois (12/2/08).

*[65] M. C. Hersam, “Preparation and characterization of high purity single-walled and double-walled carbon nanotubes,” presented orally by M. C. Hersam at the 2008 Materials Research Society Fall Meeting, Boston, Massachusetts (11/30/08).

*[66] M. C. Hersam, “Monodisperse single-walled carbon nanotubes: Processing, applications, and commercialization,” presented orally by M. C. Hersam at the Kellogg NanoAlliance Seminar Series, Evanston, Illinois (11/13/08).

*[67] M. C. Hersam, “Nanomaterials for electronics, sensing, and alternative energy,” presented orally by M. C. Hersam at the McCormick Advisory Council Meeting, Evanston, Illinois (10/10/08).

*[68] M. C. Hersam, “Alternative energy opportunities for high purity carbon nanomaterials,” presented orally by M. C. Hersam at the Joint India-US Workshop on Scalable Nanomaterials for Enhanced Energy Transport, Conversion, and Efficiency, Bangalore, India (8/19/08).

*[69] M. C. Hersam, “Size-dependent properties: Opportunities and obstacles for nanomaterials,” presented orally by M. C. Hersam at the Symposium Toward a Strategic Vision for Chemical and Biological Defense, Atlanta, Georgia (8/7/08).

*[70] M. C. Hersam, “Progress towards monodisperse carbon nanotubes,” presented orally by M. C. Hersam at the Virtual Conference on Nanoscale Science and Technology, Fayetteville, Arkansas (7/25/08).

*[71] M. C. Hersam, “High purity carbon-based nanoelectronic materials,” presented orally by M. C. Hersam at the Gordon Conference on Nanostructure Fabrication, Tilton, New Hampshire (7/16/08).

*[72] M. C. Hersam, “Preparation and characterization of monodisperse carbon-based nanomaterials,” presented orally by M. C. Hersam at the 2nd International Workshop on Metrology, Standardization, and Industrial Quality of Nanotubes, Montpellier, France (6/28/08).

[73] D. J. Comstock, J. W. Elam, M. J. Pellin, and M. C. Hersam, “Fabrication of nanopillar scanning electrochemical atomic force microscopy probes,” presented as a poster by D. J. Comstock at the 2008 AVS Prairie Chapter Meeting, Milwaukee, Wisconsin (6/9/08).

*[74] M. C. Hersam, “Probing the structure and properties of individual molecules on silicon surfaces,” presented orally by M. C. Hersam at the 52nd International Conference on Electron, Ion, and Photon Beam Technology and Nanofabrication, Portland, Oregon (5/30/08).

*[75] M. C. Hersam, “Tuning the electrical and optical properties of monodisperse carbon-based nanomaterials,” presented orally by M. C. Hersam at the 213th Electrochemical Society Meeting, Phoenix, Arizona (5/19/08).

*[76] M. C. Hersam, “Hybrid organic-inorganic nanoelectronic materials,” presented orally by M. C. Hersam at the NU-ANL-JNC Workshop on Advanced Materials, Evanston, Illinois (3/31/08).

*[77] M. C. Hersam, “Recent developments and applications of chirality-resolved single-walled carbon nanotubes,” presented orally by M. C. Hersam at the Materials Research Society Spring Meeting, Boston, Massachusetts (3/27/08).

*[78] M. C. Hersam, “Probing and manipulating surface chemistry with scanning probe microscopy,” presented orally by M. C. Hersam at the Army Research Office Organic and Inorganic Chemistry Workshop, Boston, Massachusetts (3/19/08).

*[79] M. C. Hersam, “Preparation, characterization, and applications of monodisperse single-walled carbon nanotubes,” presented orally by M. C. Hersam at the 22nd International Winterschool on Electronic Properties of Novel Materials, Kirchberg, Austria (3/6/08).

*[80] M. C. Hersam, “Tuning the electrical and optical properties of monodisperse carbon-based nanomaterials,” presented orally by M. C. Hersam at the Yonsei Global Engineering Symposium, Seoul, Korea (2/14/08).

*[81] M. C. Hersam, “Preparation and application of high purity carbon-based nanomaterials,” presented orally by M. C. Hersam at the Seoul National University Department of Physics Colloquium Series, Seoul, Korea (2/13/08).

*[82] M. C. Hersam, “Single molecule chemistry on silicon surfaces characterized by ultra-high vacuum scanning tunneling microscopy,” presented orally by M. C. Hersam at the Ajou University Molecular Science and Technology Seminar Series, Suwon, Korea (2/12/08).

*[83] M. C. Hersam, “Tuning the electrical and optical properties of monodisperse carbon-based nanomaterials,” presented orally by M. C. Hersam at the Ajou University Molecular Science and Technology Seminar Series, Suwon, Korea (2/12/08).

*[84] M. C. Hersam, “Production and application of high purity carbon-based nanomaterials,” presented orally by M. C. Hersam at the University of Illinois at Chicago Department of Mechanical and Industrial Engineering Colloquium Series, Chicago, Illinois (1/22/08).

*[85] M. C. Hersam, “Carbon nanotubes: A new form of particulate matter,” presented orally by M. C. Hersam at the Northwestern University Division of Pulmonary and Critical Care Colloquium Series, Chicago, Illinois (12/17/07).

*[86] M. C. Hersam, “Probing the structure and properties of individual molecules on silicon surfaces,” presented orally by M. C. Hersam at the University of Albany College of Nanoscale Science and Engineering Colloquium Series, Albany, New York (12/7/07).

*[87] M. C. Hersam, “Recent developments and applications of high purity carbon nanomaterials,” presented orally by M. C. Hersam at the Rensselaer Polytechnic Institute Department of Materials Science and Engineering Colloquium Series, Troy, New York (12/6/07).

*[88] M. C. Hersam, “Chirality-resolved single-walled carbon nanotubes: Processing, characterization, and applications,” presented orally by M. C. Hersam at the Materials Research Society Fall Meeting, Boston, Massachusetts (11/29/07).

[89] D. J. Comstock, J. W. Elam, J. M. Hiller, M. J. Pellin, and M. C. Hersam, “Fabrication of novel nanopillar scanning electrochemical microscopy - atomic force microscopy probes,” presented orally by D. J. Comstock at the Materials Research Society Fall Meeting, Boston, Massachusetts (11/27/07).

*[90] M. C. Hersam, “Separating carbon nanotubes by their physical and electronic structure using density gradient ultracentrifugation,” presented orally by M. C. Hersam at the FACSS Society for Applied Spectroscopy National Meeting, Memphis, Tennessee (10/18/07).

*[91] M. C. Hersam, “Multi-functional carbon-based nanoelectronic materials,” presented orally by M. C. Hersam at the Molecular Foundry Users Meeting, Berkeley, California (10/5/07).

*[92] M. C. Hersam, “Sorting single-walled carbon nanotubes by their physical and electronic structure using density differentiation,”

presented orally by M. C. Hersam at the 3rd NASA-NIST Workshop on Nanotube Measurements, Gaithersburg, Maryland (9/26/07).

*[93] M. C. Hersam, “Structure, properties, and processing of chirality-resolved single-walled carbon nanotubes,” presented orally by M. C. Hersam at the University of Arkansas at Little Rock Joint College Colloquium Series, Little Rock, Arkansas (9/14/07).

*[94] M. C. Hersam, “Characterization and manipulation of single molecule chemistry on silicon surfaces,” presented orally by M. C. Hersam at the Argonne National Laboratory Center for Nanoscale Materials Colloquium, Argonne, Illinois (9/6/07).

*[95] M. C. Hersam, “Introduction to scanning probe lithography,” presented orally by M. C. Hersam at the National Science Foundation Summer Institute on Nano Mechanics and Materials, Evanston, Illinois (7/9/07).

*[96] M. C. Hersam, “Introduction to scanning probe microscopy,” presented orally by M. C. Hersam at the National Science Foundation Summer Institute on Nano Mechanics and Materials, Evanston, Illinois (7/9/07).

*[97] M. C. Hersam, “Introduction to lithography,” presented orally by M. C. Hersam at the National Science Foundation Summer Institute on Nano Mechanics and Materials, Evanston, Illinois (7/9/07).

*[98] M. C. Hersam, “Nanoelectronic and nanophotonic materials and devices,” presented as a poster by M. C. Hersam at the Coalition for National Science Funding Exhibition, Washington, DC (6/26/07).

*[99] M. C. Hersam, “Monodisperse single-walled carbon nanotubes prepared by density gradient ultracentrifugation,” presented orally by M. C. Hersam at the European Materials Research Society Spring Meeting, Strasbourg, France (5/30/07).

*[100] M. C. Hersam, “Separations of carbon nanotubes,” presented orally by M. C. Hersam at the Oklahoma EPSCoR Annual State Conference, Stillwater, Oklahoma (5/17/07).

*[101] M. C. Hersam, “Hybrid organic/inorganic nanoelectronic materials: Characterization, processing, and applications,” presented orally by M. C. Hersam at the Center for Nanoscale Materials Workshop on Nanoelectronics, Argonne, Illinois (5/10/07).

*[102] M. C. Hersam, “Isolating monodisperse single-walled carbon nanotubes via density gradient ultracentrifugation,” presented orally by M. C. Hersam at the 211th Electrochemical Society Meeting, Chicago, Illinois (5/7/07).

*[103] M. C. Hersam, “Hybrid organic/inorganic nanomaterials: Characterization, processing, and applications,” presented orally by M. C. Hersam at the Kenyon College Department of Physics Colloquium, Gambier, Ohio (4/23/07).

*[104] M. C. Hersam, “Organic functionalization of semiconductor surfaces for molecular electronic and biosensing applications,” presented orally by M. C. Hersam at the Joint Symposium between Northwestern University and Yonsei University, Evanston, Illinois (4/13/07).

*[105] M. C. Hersam, “Sorting single-walled carbon nanotubes by their electronic structure using density gradient ultracentrifugation,” presented orally by M. C. Hersam at the Materials Research Society Spring Meeting, San Francisco, California (4/12/07).

*[106] M. C. Hersam, “Chirality-resolved single-walled carbon nanotubes,” presented orally by M. C. Hersam at the Cornell University Center for Nanoscale Systems Seminar Series, Ithaca, New York (3/29/07).

*[107] M. C. Hersam, “Structure, properties, and processing of chirality-resolved single-walled carbon nanotubes,” presented orally by M. C. Hersam at the University of Louisville Chemical Engineering Colloquium, Louisville, Kentucky (3/9/07).

*[108] M. C. Hersam, “Probing molecular electronics with scanning probe microscopy,” presented orally by M. C. Hersam at the Ajou University Molecular Science and Technology Seminar Series, Suwon, Korea (2/27/07).

*[109] M. C. Hersam, “Nanoelectronics: Device physics and fabrication technology,” presented orally by M. C. Hersam at the Ajou University Molecular Science and Technology Seminar Series, Suwon, Korea (2/26/07).

*[110] M. C. Hersam, “Introduction to nanometer scale science and technology,” presented orally by M. C. Hersam at the Ajou University Molecular Science and Technology Seminar Series, Suwon, Korea (2/26/07).

*[111] M. C. Hersam, “Purification and optical properties of biofunctionalized carbon nanotubes: Implications for multi-analyte sensing,” presented orally by M. C. Hersam at the SPIE Photonics West Meeting, San Jose, California (1/25/07).

*[112] M. C. Hersam, “Introduction to nanometer-scale science and technology,” presented orally by M. C. Hersam at the American Society for Mechanical Engineers Chicago Chapter Meeting, Evanston, Illinois (1/9/07).

*[113] M. C. Hersam, “Sorting single-walled carbon nanotubes via density gradient centrifugation,” presented orally by M. C. Hersam at the Nano Business Alliance Seminar Series, Skokie, Illinois (12/12/06).

*[114] M. C. Hersam, “Functionalized single-walled carbon nanotubes: Characterization, applications, and sorting by electronic structure,” presented orally by M. C. Hersam at the Illinois Institute of Technology Department of Chemistry Colloquium, Chicago, Illinois (12/1/06).

*[115] M. C. Hersam, “Probing molecular electronics with scanning probe microscopy,” presented orally by M. C. Hersam at the Pan-American Advanced Studies Institute Program on Nano and Biotechnology, Bariloche, Argentina (11/20/06).

*[116] M. C. Hersam, “Nanoelectronics: Device physics and fabrication technology,” presented orally by M. C. Hersam at the Pan-American Advanced Studies Institute Program on Nano and Biotechnology, Bariloche, Argentina (11/20/06).

*[117] M. C. Hersam, “Biofunctionalized single-walled carbon nanotubes: Purification, properties, and devices,” presented orally by M. C. Hersam at the AVS 53rd International Symposium, San Francisco, California (11/15/06).

[118] D. J. Comstock, M. C. Hersam, J. W. Elam, and M. J. Pellin, “Fabrication of integrated scanning electrochemical / atomic force microscopy probes by atomic layer deposition of aluminum oxide,” presented orally by D. J. Comstock at the AVS 53rd International Symposium, San Francisco, California (11/13/06).

*[119] M. C. Hersam, “High-density biomedical nanosensors,” presented orally by M. C. Hersam at the Lifelong Learners Seminar Series, Chicago, Illinois (11/8/06).

*[120] M. C. Hersam, “Electronic and optical devices based on purified biofunctionalized carbon nanotubes,” presented orally by M. C. Hersam at the 210th Meeting of the Electrochemical Society, Cancun, Mexico (10/31/06).

*[121] M. C. Hersam, “Functionalized carbon nanotubes: Purification, characterization, and applications,” presented orally by M. C. Hersam at the 2006 International Institute for Nanotechnology Symposium, Evanston, Illinois (10/11/06).

*[122] M. C. Hersam, “Purification and optical properties of biofunctionalized carbon nanotubes,” presented orally by M. C. Hersam at the ASME International Conference on Manufacturing Science and Technology, Ypsilanti, Michigan (10/10/06).

*[123] M. C. Hersam, “Introduction to nanometer scale science and technology,” presented orally by M. C. Hersam at the Harold Washington College Nanoscience Seminar Series, Chicago, Illinois (10/5/06).

*[124] M. C. Hersam, “Probing chemistry and electronic structure at the single molecule level with scanning tunneling microscopy,” presented orally by M. C. Hersam at the Tufts University Department of Chemistry Colloquium, Medford, Massachusetts (10/3/06).

*[125] M. C. Hersam, “Electrical contacts at the nanometer scale,” presented orally by M. C. Hersam at the 52nd IEEE Holm Symposium, Montreal, Canada (9/27/06).

*[126] M. C. Hersam, “Probing the dynamics of individual molecules on silicon surfaces with ultra-high vacuum scanning tunneling microscopy,” presented orally by M. C. Hersam at the ACS Fall Meeting, San Francisco, California (9/11/06).

*[127] M. C. Hersam, “Functionalized carbon nanotubes: Purification, characterization, and device applications,” presented orally by M. C. Hersam at the Center for Quantum Devices Seminar Series, Evanston, Illinois (8/31/06).

*[128] M. C. Hersam, “Probing molecular electronics with scanning probe microscopy,” presented orally by M. C. Hersam at the National Science Foundation Summer Institute on Micro and Nano Devices with Applications to Biology and Nanoelectronics, Evanston, Illinois (8/10/06).

*[129] M. C. Hersam, “Nanoelectronics: Device physics and fabrication technology,” presented orally by M. C. Hersam at the National Science Foundation Summer Institute on Micro and Nano Devices with Applications to Biology and Nanoelectronics, Evanston, Illinois (8/10/06).

*[130] M. C. Hersam, “Ultra-high vacuum scanning tunneling microscopy studies of single molecules on semiconductor surfaces,” presented orally by M. C. Hersam at the International Conference on Nanoscience and Technology, Basel, Switzerland (8/2/06).

*[131] M. C. Hersam, “Assessing the prospects and limitations of silicon-based molecular electronics with ultra-high vacuum scanning tunneling microscopy,” presented orally by M. C. Hersam at the Molecular Conductivity and Sensor Workshop, Charlottesville, Virginia (7/27/06).

[132] D. J. Comstock, M. C. Hersam, J. W. Elam, and M. J. Pellin, “Fabrication of conductive probes for scanning electrochemical microscopy using atomic layer deposition techniques,” presented as a poster by J. W. Elam at the AVS 6th International Conference on Atomic Layer Deposition, Seoul, South Korea (7/27/06).

*[133] M. C. Hersam, “Introduction to nanoelectronics,” presented orally by M. C. Hersam at the ASME Nano Training Bootcamp, St. Paul, Minnesota (7/13/06).

[134] D. J. Comstock, J. W. Elam, M. J. Pellin, and M. C. Hersam, “Fabrication of integrated scanning electrochemical atomic force microscopy probes by atomic layer deposition of aluminum oxide,” presented orally by D. J. Comstock at the AVS Prairie Chapter Regional Meeting, Naperville, Illinois (6/12/06).

*[135] M. C. Hersam, “Probing organic chemistry on silicon surfaces at the single molecule level with ultra-high vacuum scanning tunneling microscopy,” presented orally by M. C. Hersam at the University of California at Riverside Chemistry Department Colloquium, Riverside, California (6/7/06).

*[136] M. C. Hersam, “Nanomaterials for biomedical sensing,” presented orally by M. C. Hersam at the Symposium on Bionanotechnology for Medical Applications, Chicago, Illinois (5/8/06).

*[137] M. C. Hersam, “Assessing the prospects and limitations of silicon-based molecular electronics with ultra-high vacuum scanning tunneling microscopy,” presented orally by M. C. Hersam at the University of Illinois at Urbana-Champaign Materials Science and Engineering Department Colloquium, Urbana, Illinois (4/17/06).

*[138] M. C. Hersam, “Atomic resolution patterning of organosilicon heteromolecular nanostructures using feedback controlled lithography,” presented orally by M. C. Hersam at the ACS Spring Meeting, Atlanta, Georgia (3/26/06).

*[139] M. C. Hersam, “Molecular-scale patterning and characterization of organic structures on silicon,” presented orally by M. C. Hersam at the Joint International Conference on New Phenomena in Mesoscopic Systems and Surfaces and Interfaces of Mesoscopic Devices, Maui, Hawaii (12/2/05).

*[140] M. C. Hersam, “Probing silicon-molecule junctions with scanning tunneling microscopy,” presented orally by M. C. Hersam at the Materials Research Society Fall Meeting, Boston, Massachusetts (11/29/05).

*[141] M. C. Hersam, “Directed assembly and characterization of organosilicon nanostructures using scanning tunneling microscopy,” presented orally by M. C. Hersam at the International Symposium on Surface Science and Nanotechnology, Saitama, Japan (11/16/05).

*[142] M. C. Hersam, “Nanoelectronics: Device physics and fabrication technology,” presented orally by M. C. Hersam at the NanoCommerce/SEMI NanoForum, Chicago, Illinois (10/31/05).

*[143] M. C. Hersam, “Hybrid organic/inorganic materials at the nanometer scale,” presented orally by M. C. Hersam at the Golden Jubilee of Materials Science and Engineering, Evanston, Illinois (10/28/05).

*[144] M. C. Hersam, “Separation of single-walled carbon nanotubes by diameter using density gradient centrifugation,” presented orally by M. C. Hersam at the FACSS 51st International Conference on Analytical Sciences and Spectroscopy, Quebec City, Canada (10/10/05).

*[145] M. C. Hersam, “Hybrid organic/inorganic nanomaterials: Characterization, processing, and potential applications,” presented orally by M. C. Hersam at the University of Pennsylvania Materials Science and Engineering Colloquium, Philadelphia, Pennsylvania (9/29/05).

*[146] M. C. Hersam, “Purification and optical properties of biofunctionalized carbon nanotubes,” presented orally by M. C. Hersam at the Materials Science and Technology 2005 Conference, Pittsburgh, Pennsylvania (9/28/05).

*[147] M. C. Hersam, “Probing single molecule charge transport on silicon surfaces using scanning tunneling microscopy,” presented orally by M. C. Hersam at the Bat Sheva Seminar on Electron Transport in Molecular Junctions, Mizpe Hayamim, Israel (9/18/05).

*[148] M. C. Hersam, “Observing and manipulating single molecule motion using scanning tunneling microscopy,” presented orally by M. C. Hersam at the 230th American Chemical Society National Meeting, Washington, DC (8/29/05).

*[149] M. C. Hersam, “Introduction to nanoscale science and technology,” presented orally by M. C. Hersam at the Khon Kaen University School of Pharmacy Colloquium, Khon Kaen, Thailand (8/10/05).

*[150] M. C. Hersam, “Single molecule sensing, characterization, and actuation,” presented orally by M. C. Hersam at the International Materials Research and Nanotechnology Workshop, Khon Kaen, Thailand (8/8/05).

*[151] M. C. Hersam, “Probing silicon-based molecular electronics with scanning tunneling microscopy,” presented orally by M. C. Hersam at the Molecular Conduction and Sensing Workshop, West Lafayette, Indiana (7/29/05).

*[152] M. C. Hersam, “Introduction to nanoelectronics,” presented orally by M. C. Hersam at the ASME Nano Training Bootcamp, Washington, D.C. (7/14/05).

*[153] M. C. Hersam, “Probing silicon-based molecular electronics with scanning tunneling microscopy,” presented orally by M. C. Hersam at the Columbia University Nanoscale Science and Engineering Center Seminar Series, New York, New York (4/27/05).

*[154] M. C. Hersam, “Introduction to nanometer scale science and technology,” presented orally by M. C. Hersam at the American Institute of Chemical Engineering Chicago Section Symposium, Chicago, Illinois (4/20/05).

*[155] M. C. Hersam, “Probing electronic properties at the single molecule level on silicon surfaces,” presented orally by M. C. Hersam at the Yale University Solid State and Optics Seminar Series, New Haven, Connecticut (4/13/05).

Number of Presentations: 155.00

Non Peer-Reviewed Conference Proceeding publications (other than abstracts):

Received Paper

TOTAL:

Number of Non Peer-Reviewed Conference Proceeding publications (other than abstracts):

Peer-Reviewed Conference Proceeding publications (other than abstracts):

Received Paper

TOTAL:

Number of Peer-Reviewed Conference Proceeding publications (other than abstracts):

(d) Manuscripts

Received	Paper
2009/12/30 18	8 M. D. Irwin, J. Liu, B. J. Leever, M. C. Hersam, M. F. Durstock, and T. J. Marks. Consequences of anode interfacial layer deletion. HCl-treated ITO in P3HT:PCBM-based bulk-heterojunction organic photovoltaic devices, (08 2009)
2009/12/30 18	7 D. J. Comstock, J. W. Elam, and M. C. Hersam. Integrated ultramicroelectrode-nanopipette probe for concurrent scanning electrochemical microscopy and scanning ion conductance microscopy, (12 2009)

TOTAL: 2

Number of Manuscripts:

Books

Received	Paper

TOTAL:

Patents Submitted

[1] "Nanoscale, spatially-controlled Ga doping of undoped transparent conducting oxide films," N. E. S. Cortes, T. J. Marks, and M. C. Hersam, U.S. Patent application filed 6/22/09.

Patents Awarded

[1] "System and methods of laser assisted field induced oxide nanopatterning," L. S. C. Pingree and M. C. Hersam, U.S. Patent #7,976,765 issued 7/12/11.

Awards

[1] AVS Prairie Chapter Award for Outstanding Research, 2011
[2] Teacher of the Year in the Department of Materials Science and Engineering, 2010
[3] Materials Research Society Outstanding Young Investigator Award, 2010
[4] SES Research Young Investigator Award, Electrochemical Society, 2010
[5] Senior Member, Institute of Electrical and Electronics Engineers, 2009
[6] Teacher of the Year in the Department of Materials Science and Engineering, 2007
[7] Young Alumni Achievement Award, ECE Department, UIUC, 2007
[8] AVS Peter Mark Award, 2006
[9] TMS Robert Lansing Hardy Award, 2006
[10] Chicago Area Undergraduate Research Symposium Faculty Research Award, 2006
[11] Presidential Early Career Award for Scientists and Engineers, 2005
[12] Alfred P. Sloan Research Fellowship, 2005

Graduate Students

NAME	PERCENT_SUPPORTED	Discipline
David Comstock	0.50	
Albert Lipson	0.50	
FTE Equivalent:	**1.00**	
Total Number:	**2**	

Names of Post Doctorates

NAME	PERCENT_SUPPORTED
FTE Equivalent:	
Total Number:	

Names of Faculty Supported

NAME	PERCENT_SUPPORTED	National Academy Member
Mark Hersam	0.06	
FTE Equivalent:	**0.06**	
Total Number:	**1**	

Names of Under Graduate students supported

NAME	PERCENT_SUPPORTED	Discipline
Ryan Ginder	0.20	Materials Science and Engineering
Alexander Antaris	0.20	Electrical Engineering
FTE Equivalent:	**0.40**	
Total Number:	**2**	

Student Metrics

This section only applies to graduating undergraduates supported by this agreement in this reporting period

The number of undergraduates funded by this agreement who graduated during this period:	2.00
The number of undergraduates funded by this agreement who graduated during this period with a degree in science, mathematics, engineering, or technology fields:.....	2.00
The number of undergraduates funded by your agreement who graduated during this period and will continue to pursue a graduate or Ph.D. degree in science, mathematics, engineering, or technology fields:.....	2.00
Number of graduating undergraduates who achieved a 3.5 GPA to 4.0 (4.0 max scale):	2.00
Number of graduating undergraduates funded by a DoD funded Center of Excellence grant for Education, Research and Engineering:	0.00
The number of undergraduates funded by your agreement who graduated during this period and intend to work for the Department of Defense	0.00
The number of undergraduates funded by your agreement who graduated during this period and will receive scholarships or fellowships for further studies in science, mathematics, engineering or technology fields:	2.00

Names of Personnel receiving masters degrees

NAME
Total Number:

Names of personnel receiving PHDs

NAME	
David Comstock	
Total Number:	**1**

Names of other research staff

NAME	PERCENT_SUPPORTED
FTE Equivalent:	
Total Number:	

Sub Contractors (DD882)

Inventions (DD882)

5 **System and methods of laser assisted field induced oxide nanopatterning**

Patent Filed in US? (5d-1) Y

Patent Filed in Foreign Countries? (5d-2) N

Was the assignment forwarded to the contracting officer? (5e) N

Foreign Countries of application (5g-2):

5a: Liam S. C. Pingree

5f-1a: Northwestern University

5f-c: 2220 Campus Drive

Evanston IL 60208

5a: Mark C. Hersam

5f-1a: Northwestern University

5f-c: 2220 Campus Drive

Evanston IL 60208

Scientific Progress

See Attachment

Technology Transfer

Army Research Office Young Investigator Program
Presidential Early Career Award for Scientists and Engineers
"Nanoscale Probing of Electrical Signals in Biological Systems"
Contract Number: W911NF-05-1-0177
Final Report
Period covered: 4/5/05 – 11/4/11

PI: Mark C. Hersam, Professor
Department of Materials Science and Engineering
Department of Chemistry
Northwestern University
http://www.hersam-group.northwestern.edu/

Scientific Progress and Accomplishments

1. Scanning Ion Conductance Microscopy of Electrochemically Active Electrodes

Prior work has established scanning ion conductance microscopy (SICM) as an important technique for nanoscale characterization in aqueous electrolytes. SICM is an entirely non-contact method, which provides distinct advantages for topographical imaging of delicate structures such as biological cells in liquids. SICM can also be combined with scanning electrochemical microscopy (SECM) to add further electrochemical capabilities beyond topographic mapping. Since SICM directly measures ion currents through a nanoscale pipette, it is well suited for simultaneous imaging of topography and ion currents, as has been previously shown for porous membranes. In order to obtain these spatially resolved ion currents, the SICM is implemented in a loose patch clamp geometry where the pipette is brought close to the sample to form a low resistance seal. Over the past year, we have employed SICM as a tool for concurrently imaging the topography and local Li^+ ion currents on battery electrode materials. This in situ characterization reveals the evolution of spatial inhomogeneities in the structure and electrochemical activity of the substrate as a function of lithiation state, thus providing unique nanoscale insight into the operation of Li-ion batteries.

Since SICM is a technique originally developed for biological samples, many modifications were made to the SICM apparatus to enable imaging of battery electrodes in situ. **Figure 1** shows a schematic of the SICM configuration used in this study. The electrically grounded sample is mounted in a petri dish, which is then filled with the battery electrolyte. A glass pipette, pulled to the desired diameter, is filled with the same electrolyte, and a lithiated tin wire is placed inside. Lithiated tin is used as the source of Li^+ ions instead of lithium metal as similarly sized lithium wire was not mechanically robust enough to survive the pipette insertion process.

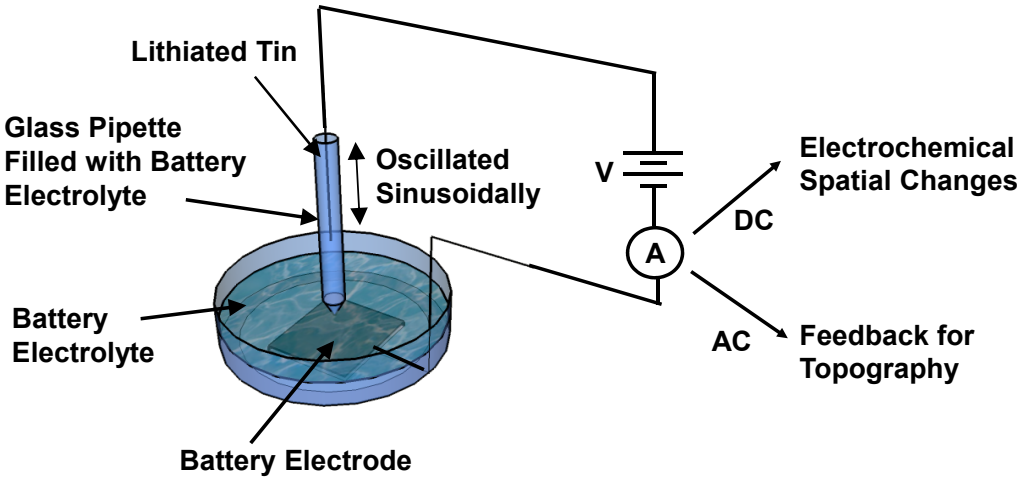

Figure 1. Schematic diagram of the in situ Li-ion battery SICM configuration. The entire apparatus is housed inside of an argon filled glovebox, which permits the use of electrolytes that are employed in actual Li-ion batteries.

Once the pipette is lowered into the electrolyte in the petri dish, a Li^+ ion current flows from the tip into the sample. As the tip approaches the sample, the seal resistance increases between the pipette and the electrode material that is not directly beneath the tip. Since the majority of the original current is supplied by the surrounding electrode material, the current at a constant voltage decreases as the tip approaches the sample. When the tip is oscillated vertically, the magnitude of the alternating current (AC) at the driving frequency monotonically increases as the tip approaches the sample. In this manner, the magnitude of the AC current can be used as the feedback signal to maintain a constant tip-sample spacing. Since a constant tip-sample spacing implies a constant average seal resistance, the current remains constant between the pipette and the sample beyond the local region of the tip. Consequently, changes to the overall current during scanning are predominantly attributed to spatial variations in the ionic current.

Spatial inhomogeneity in the ionic current can be caused by a number of factors. Ideally, current should be generated equally throughout the volume of the electrode material. In this case, the local ionic current will be proportional to the electrode material thickness, implying a direct relationship between sample thickness and ionic current. On the other hand, if a region of the electrode is inactive or less active due to poor electrical contact to the current collector, a reduction in current can be expected. Similarly, barriers to lithiation such as the formation of a relatively impervious solid electrolyte interphase (SEI) layer will also reduce the local ionic current. In a real battery electrode, the ionic current will be a convolution of these effects.

To determine the relative importance of these potentially competing contributions to the ionic current, a variety of test samples were characterized with SICM. Initially, silicon nanoparticles mixed with poly(vinylidene difluoride) (PVDF) deposited on copper foil were prepared to illustrate current contrast based on sample thickness. The drop-casting conditions were adjusted to ensure high surface roughness and corresponding variability in sample thickness. The resulting SICM topography and current images are shown in **Figure 2**. The measured current is higher over topographically protruding regions since all of the nanoparticles throughout the sample thickness can participate in lithiation. Reduced current is also observed around the protruding features, which is likely due to a local depletion in Si nanoparticles as they are incorporated into the larger agglomerate during drop-casting.

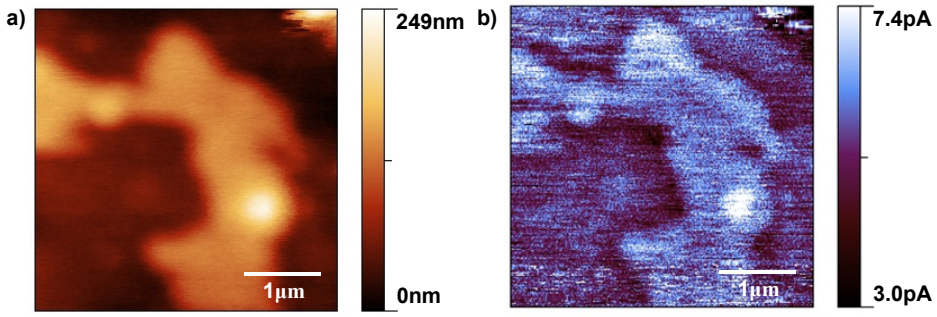

Figure 2. SICM (a) topography image and (b) DC current map of silicon nanoparticles and PVDF deposited via drop-casting on copper foil.

To directly compare electrochemically active and inactive materials, tin stripes were fabricated on a copper thin film on glass. The resulting SICM images of this lithographically defined sample are shown in **Figure 3**. A clear increase in current is detected over the regions of the tin stripes as expected. In particular, **Figure 3c** shows the extracted profile perpendicular to the stripe, which has been averaged over 128 pixels. In addition to the increased current in the flat region of the tin stripe, imaging artifacts characteristic of cross-talk between topography and current are observed to the left and right of the stripe. Since the fast scan direction is from left to right, the pipette approaches a steep incline on the left side and a steep drop on the right side of the tin stripes. The finite response time of the feedback system implies that the tip is closer to the surface than the setpoint on the left side and further away on the right, leading to the observed drop in current on the left and slight increase in current on the right. Increasing data acquisition time (i.e., reducing scan speed) allows this effect to be minimized.

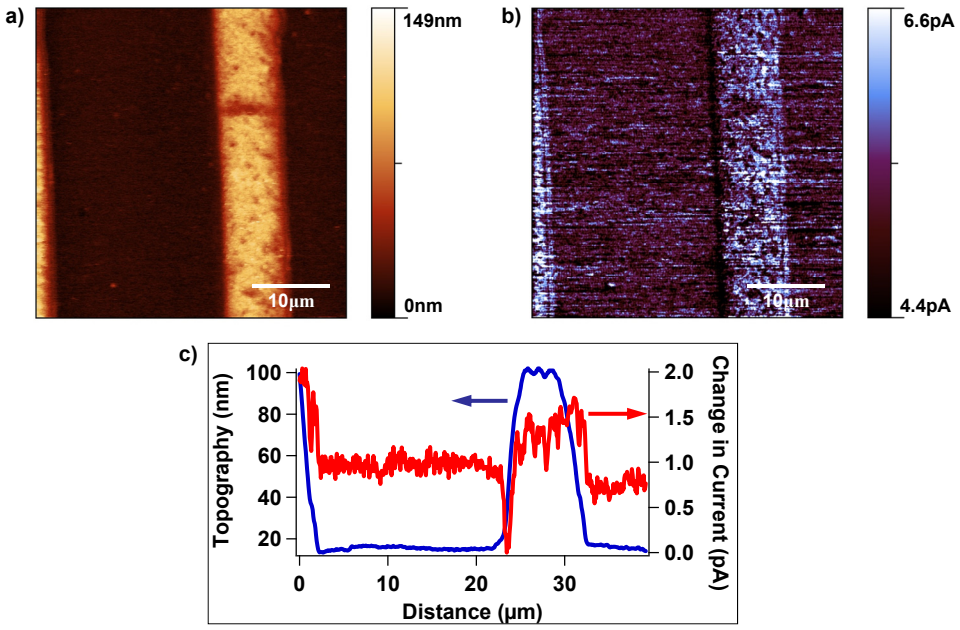

Figure 3. SICM of tin stripes on 60 nm of copper on glass: (a) topography image, (b) DC current map, and (c) extracted profile averaged over 128 pixels parallel to the stripes.

To explore a more realistic battery electrode, a tin thin film was evaporated on a copper thin film on glass. These as-deposited films naturally possess topographical corrugation exceeding 10 nm as can be seen in **Figure 4a**. The contrast in the corresponding SICM current map in **Figure 4b** is dominated by thickness variations in a similar fashion to the silicon nanoparticle composite shown in **Figure 2**. After partial lithiation of 24 $\mu Ahcm^{-2}$ at 24 $\mu A\ cm^{-2}$, significant structural changes are observed in **Figures 4c** and **4d**. In particular, local regions have undergone clear increases in topography, likely due to catalytic decomposition of the electrolyte. Overall, the current has increased over these features, which is consistent with their preferential growth.

A closer evaluation of these images provides further insight into the growth process. Extracted profiles along the yellow and green lines of **Figures 4c** and **4d** are shown in **Figure 5**. In particular, **Figure 5a** shows a drop in current that is apparent around the topographically protruding feature. This peripheral reduction in current suggests an SEI that partially seals regions around the growing features, thereby concentrating ionic current. The profile in **Figure 5b** demonstrates that topographically high features do not necessarily correlate with regions of increased current. For example, the feature indicated by the black arrow has a similar topographic height to the other protruding features, but the corresponding current is only as high as regions in the background. This observation suggests that the growing film can eventually block the tin electrode underneath such that the electrolyte can no longer access it and catalytically decompose. Once the catalytic decomposition has ended, the current will be due to lithiation and normal SEI formation as is seen in the background.

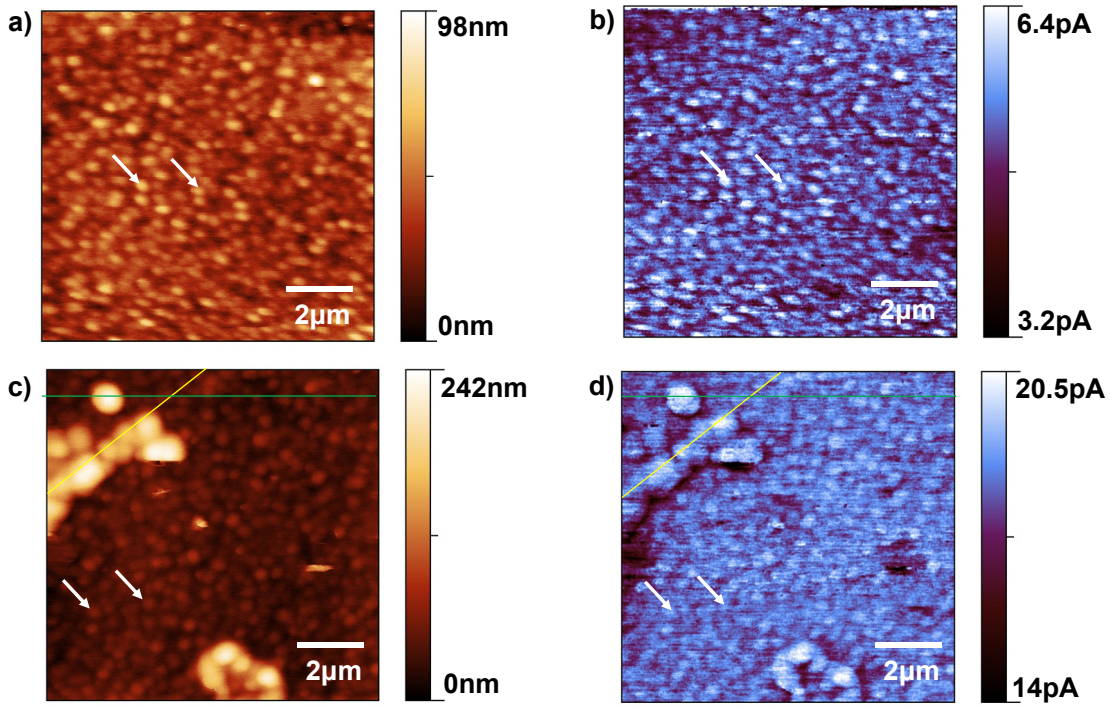

Figure 4. SICM (a,c) topography and (b,d) DC current images of a 60 nm thick tin thin film deposited on a 60 nm thick copper thin film on glass (a,b) before lithiation and (c,d) after 24$\mu Ahcm^{-2}$ lithiation.

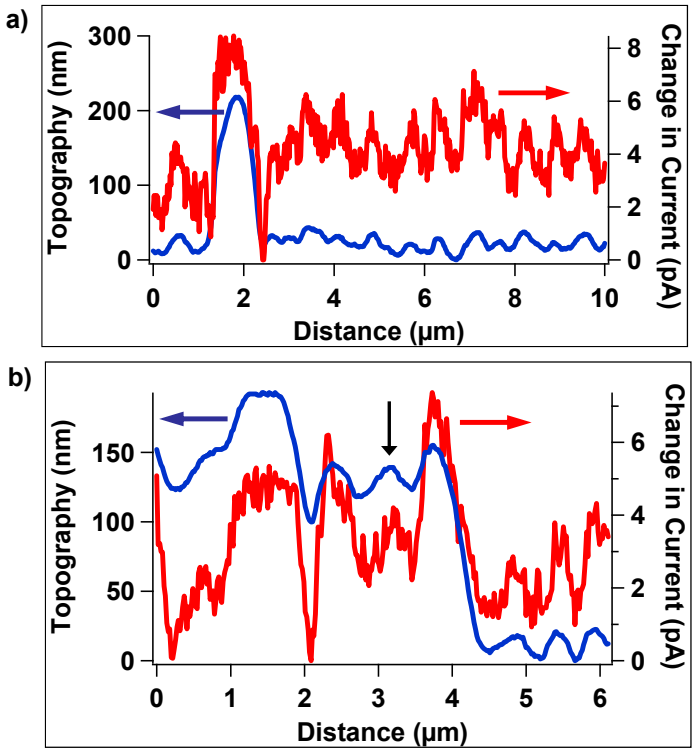

Figure 5. Extracted profiles averaged over 8 pixels wide from **Figures 4c** and **4d** for the (a) green line and (b) yellow line.

In summary, it has been demonstrated that SICM is an effective in situ technique for studying both the topography and electrochemistry of battery electrode materials at the nanoscale. Correlated topographic and current mapping of test structures reveals a number of factors that lead to spatial inhomogeneities including thickness of the active battery material and barriers to lithiation including the evolution of the SEI. Subsequent measurements on tin electrodes provide a nanoscale picture of catalytic decomposition of the electrolyte where an SEI is observed to form around electrode regions that rapidly grow during lithiation. In addition, the lithiation process can induce local film growth to the point where further electrolyte decomposition is suppressed. Overall, this work establishes the unique capabilities of SICM as an situ tool for probing spatial inhomogeneities in topography and electrochemistry in battery electrodes, thus providing new characterization data that can inform ongoing efforts to understand and improve the capacity, lifetime, and safety of lithium ion battery technology.

2. Quantification of SECM-SICM in Both DC and AC Modes

In recent years, scanning ion conductance microscopy (SICM) has emerged as a versatile noncontact imaging tool. As such, SICM can be applied to numerous biophysical systems, including proteins in cell membranes, suspended artificial membranes, ionic conductivity of porous membranes, and mechanical properties of living cells. In addition, the capabilities of SICM have been extended by integrating complementary techniques, including confocal microscopy, scanning near field optical microscopy (SNOM), and patch clamping. These auxiliary measurements provide additional information about the sample that is correlated with

the surface topography detected by SICM imaging. Despite these impressive advancements in SICM, it remains insensitive to electrochemical properties. Spatial mapping of electrochemistry is commonly achieved by scanning electrochemical imaging (SECM) and has been widely used in the study of electrode surfaces, membrane transport, and biological systems. In previous work, we advanced the capabilities of SICM for electrochemical imaging by developing and qualitatively demonstrating a nanopipette probe with an integrated ultramicroelectrode (UME) for concurrent SICM and SECM imaging. Over the past funding period, we have expanded this effort by performing quantitative SECM-SICM in both DC and AC modes.

Approach curves confirm both the feedback response of the integrated UME as it approaches a surface and the independence of the ion and redox current signals. **Figure 6** and **Figure 7** show the variations in the DC and AC components of the ion and redox currents on approach to a conducting gold surface and an insulating Teflon surface, respectively. In both cases, the DC currents are normalized with respect to their values measured far from the surface.

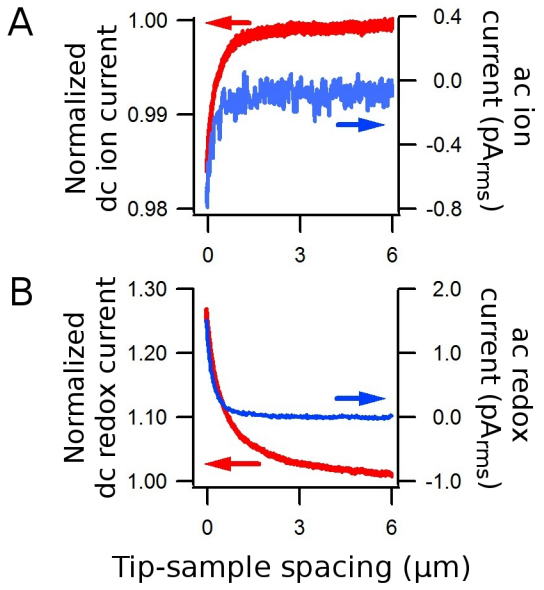

Figure 6. Approach curves to a conducting gold surface collected in 10 mM $Ru(NH_3)_6^{3+}$ with 100 mM KNO_3 supporting electrolyte. (A) Normalized DC ion current and AC ion current response. (B) Normalized DC redox current and AC redox current response.

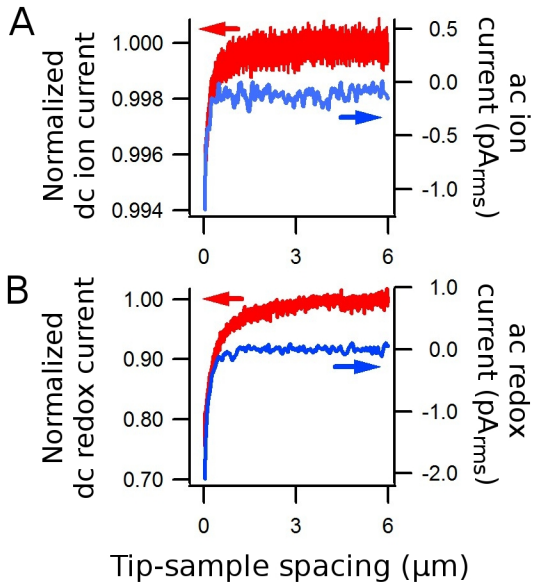

Figure 7. Approach curves to an insulating Teflon surface collected in 10 mM $Ru(NH_3)_6^{3+}$ with 100 mM KNO_3 supporting electrolyte. (A) Normalized DC ion current and AC ion current response. (B) Normalized DC redox current and AC redox current response.

The DC ion current exhibits similar behavior on approach to either surface. This observation is consistent with the SICM feedback, which depends solely on the hindered diffusion of ionic species to the nanopipette tip and is substrate independent. The AC ion current is also consistent with expectations, with an increased AC component upon approach. At large tip-sample distances, the ion current is unperturbed by the relatively small oscillation amplitude of the probe. However, as the probe approaches the surface and the oscillation amplitude become significant relative to the tip-sample spacing, this ac component increases in magnitude.

On the other hand, the redox current exhibits substrate dependent behavior on approach to conducting and insulating surfaces, consistent with the SECM feedback mechanism. As the integrated UME approaches a conducting gold surface, the DC current increases due to recycling of the UME-generated species. Conversely, as the probe approaches an insulating Teflon surface, the DC current decreases due to hindered diffusion to the UME. Similarly, the AC current also depends upon surface conductivity. Like the ion current, the redox current has no AC component at large tip-sample spacings and increases on approach to the surface. However, the AC redox current response to conducting and insulating surfaces are 180° out of phase. This phase shift can be explained by approximating the AC response as the derivative of the DC response. Positive feedback over conducting surfaces results in increased DC current and positive AC response, while negative feedback over insulating surfaces results in decreased DC current and negative AC response.

The AC redox current has significant advantages over the DC redox current as an electrochemical imaging signal. As shown in **Figure 6** and **Figure 7**, the AC signal is more surface-sensitive than the DC signal, with variations occurring at smaller tip-sample spacings relative to the DC signal. Furthermore, the AC signal eliminates the large DC offset current associated with the steady-state response of the UME, making small variations in the ac current easier to detect than small variations in the dc current. This effect has implications for the probe

fabrication as well. With DC current, any defects in the probe's insulating film produce an increased DC offset current, which complicates small signal detection. However, the AC current will remain insensitive to many of these defects, as defects far from the tip will be too far from the surface to generate an AC response. This reduced sensitivity to defects is useful, as the deposition of a high-quality, pinhole free insulating film is one of the primary challenges in fabricating SECM probes.

3. Templating Iridium Oxide Nanostructured Electrodes in AAO Membranes

Iridium oxide (IrOx) has been studied and utilized for a wide range of applications including electrochromic devices, pH sensing, and neural stimulation. IrOx is particularly well-suited for neural stimulation due to the large charge storage capacities associated with faradaic reactions between Ir^{3+} and Ir^{4+} redox states within the oxide. Furthermore, IrOx is both biocompatible and corrosion resistant, which are additional requirements for neural stimulation electrodes.

IrOx synthesis has been demonstrated by a number of strategies. Among the most common is the formation of activated IrOx films (AIROFs) by repeated potential cycling or pulsing of Ir metal in acid or phosphate-buffered electrolytes. IrOx films have also been synthesized by a number of deposition strategies, including sputtering and electrodeposition. With all synthesis strategies, control of the film morphology is particularly important, as increased film porosity has been found to enhance charge storage capacity in both AIROFs and sputtered IrOx films.

In this work, we demonstrate an alternative scheme for synthesizing morphologically controlled Ir films that enables nanoporous AIROFs with enhanced charge storage capacity. This approach utilizes atomic layer deposition (ALD) of a thin conformal Ir film into a nanoporous anodized aluminum oxide (AAO) template. AAO templates consist of hexagonally-ordered pores with controlled pore spacings and diameters and have been widely used to prepare nanoporous materials. ALD is a deposition technique utilizing iterative, self-limiting surface reactions to deposit thin films in a monolayer-by-monolayer fashion that enables films with precise thickness and compositional control, high conformality, and uniform infiltration of porous templates. Detailed synthetic procedures and thorough experimental characterization are presented below, thus establishing the advantages of nanoporous AIROFs for charge storage and pH sensing applications.

AAO templates consisting of 350 nm diameter, 18 μm long pores with 425 nm spacing were prepared using a two-step anodization procedure. Anodizations were conducted at 170 V in 0.3 M H_3PO_4 at 5° C and exhibited a growth rate of 0.3 μm/min. Following anodization, pores were widened by etching in 10 wt% H_3PO_4 at 35°C for 1 hour.

Flat and nanoporous Ir films were prepared by ALD onto glass and AAO templates, respectively. Ir ALD was conducted in a viscous flow reactor maintained at a pressure of ~1 Torr under a flow of 130 sccm N_2 (99.999% purity) carrier gas and a temperature of 300°C. After loading into the reactor, all substrates were thermally equilibrated for 10 min and then cleaned *in situ* by exposure to 10% ozone in 400 sccm O_2 for 10 min. A 20 Å Al_2O_3 film was then deposited as a nucleation layer by iterative exposures of trimethylaluminum and H_2O. Ir films were then deposited by iterative exposures of iridium(III) acetylacetonate ($Ir(acac)_3$), maintained within a stainless steel bubbler at a 170° C, and O_2. Ir ALD was conducted with 5-10

sec $Ir(acac)_3$ exposures and 2 sec O_2 exposures, with each exposure followed by a 5 sec N_2 purge. All Ir films were deposited for 600 cycles and were ~27 nm thick.

Both flat and nanoporous Ir films were electrochemically activated to form AIROFs. For all electrochemical measurements, electrical contact was made to the films with Ag paint and the films were masked with a chemically-resistant vinyl masking tape to define a 0.125" diameter electrode. The AIROFs were prepared by 200 cycles of potential cycling in 0.1 M H_2SO_4 between –0.7 and 0.8 V vs. mercury/mercurous sulfate electrode (MSE) at a scan rate of 100 mV/s. Immediately following activation, the AIROFs were characterized by cyclic voltammetry (CV) in 1 M H_2SO_4 between –0.7 and 0.8 V vs. MSE at a scan rate of 100 mV/s. The cathodal charge storage capacity (CSC_c), which provides a measure of the total charge stored within the IrOx film and available for a stimulation pulse, was determined by CV between –0.6 and 0.8 V vs. Ag/AgCl in phosphate-buffered saline solution (22 mM NaH_2PO4, 81 mM Na_2HPO4, and 130 mM NaCl). The CSC_c was calculated as the time integral of the negative current over a complete CV cycle.

Potentiometric pH sensing with the AIROFs was assessed by measuring the open circuit voltage vs. saturated calomel electrode (SCE) in commercial buffer solutions ranging in pH from 2 to 10. Samples for pH testing were activated for 200 cycles with the final activation cycle ending at 0.8 V. The sample was then immersed in H_2O for at least 12 hours prior to pH testing.

The nanoporous Ir metal films prepared by ALD into AAO templates are shown in **Figure 8**. As is characteristic of ALD films, the Ir film conformally coats both the top and internal surfaces of the nanoporous template. Additionally, cross-sectional images demonstrate that the infiltration depth of Ir within the template is controlled by the $Ir(acac)_3$ exposure time, with 5 and 10 sec exposure times resulting in infiltration depths of 2.2 and 9 μm, respectively. Additionally, as shown in **Figure 8E**, the nanoporous Ir films exhibit enhanced faradaic currents associated with hydrogen adsorption/desorption relative to flat Ir films. These enhanced currents confirm the enhanced surface area of the nanoporous Ir film and its suitability for subsequent activation.

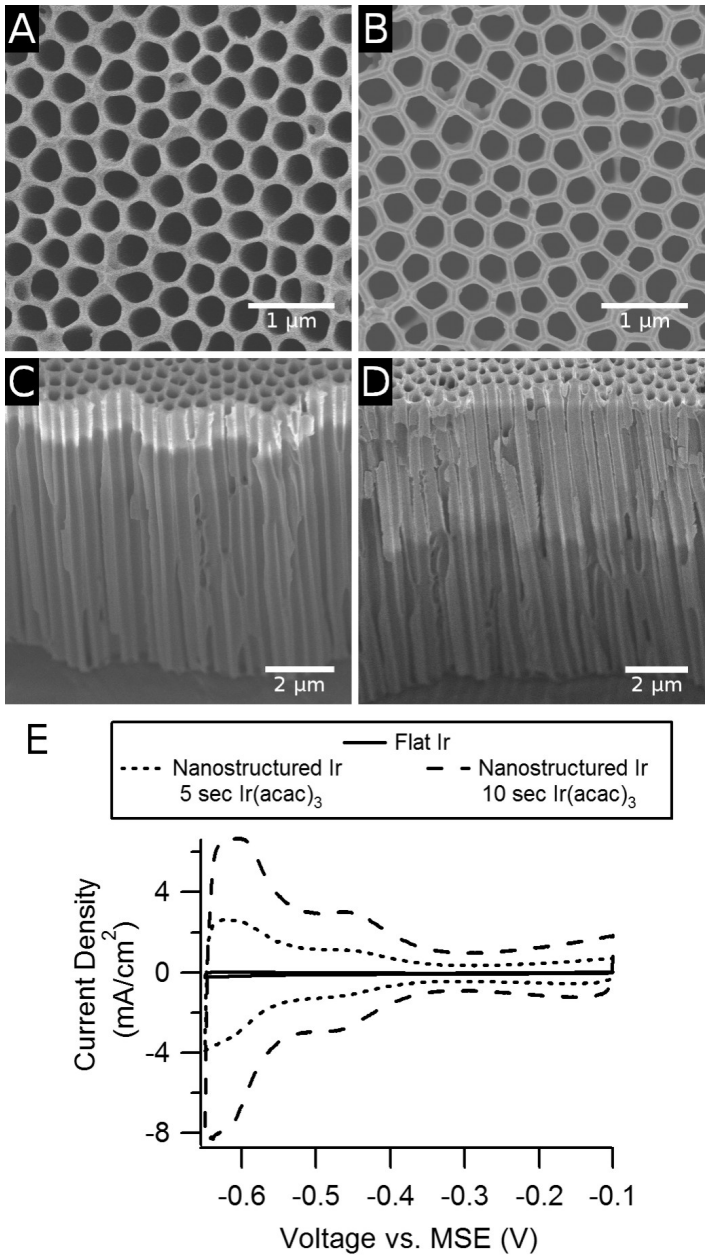

Figure 8. SEM images of the top surface of the AAO template A) before Ir ALD and B) after 600 cycles of Ir ALD. Cross-sectional SEM images of AAO templates with a 600 cycle Ir ALD film deposited with C) 5 sec $Ir(acac)_3$ exposures and D) 10 sec $Ir(acac)_3$ exposures. E) CV in 1 M H_2SO_4 of flat and nanoporous Ir films demonstrating the surface area enhancement of the nanoporous films.

Nanoporous AIROFs are prepared by potential cycling in 0.1 M H_2SO_4. As shown in **Figure 9A**, there is significant volume expansion associated with the conversion of Ir to IrOx during activation. While such volume expansion occurs with all AIROF schemes, this nanoporous AIROF synthesis scheme is advantageous in that the volume expansion can be accommodated by appropriately selecting the template dimensions. In comparison, other strategies for depositing Ir films with enhanced porosity, such as sputtering, are only capable of small-scale porosity with pores on the order of 20 nm. Based upon the observed volume

expansion, such small-scale porosity will be completely eliminated upon conversion to IrOx. This behavior was confirmed in our lab, with a 90 nm diameter nanoporous Ir film exhibiting near complete pore occlusion after 100 activation cycles. However, by appropriately selecting large diameter porous templates, as in this work, thicker Ir films and more extensively activated IrOx films can be achieved while retaining the porosity necessary to maintain electrolyte access to the large internal surface area of the nanoporous AIROF.

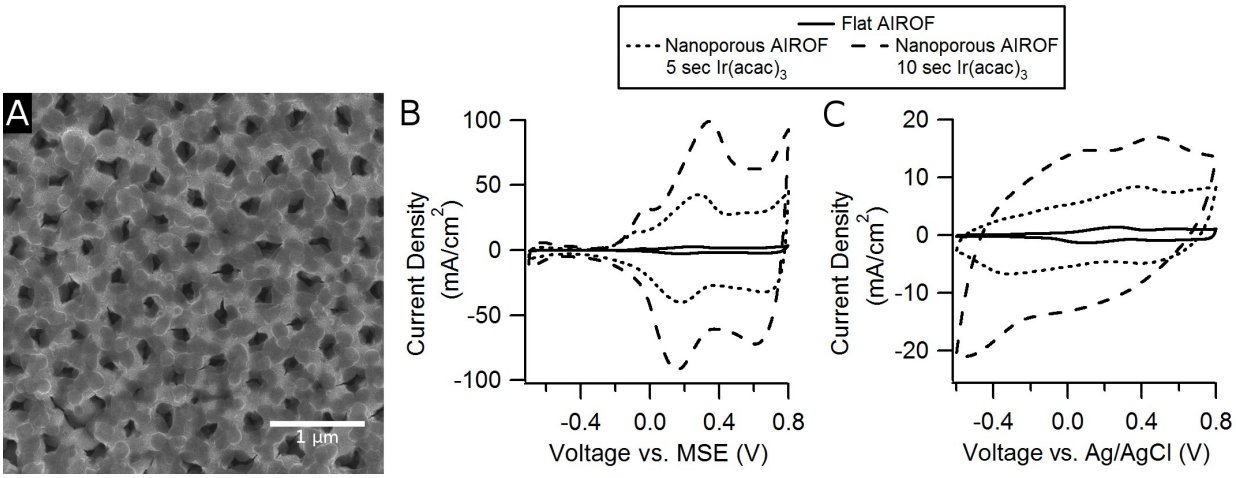

Figure 9. A) SEM image of the top surface of the AAO template following 200 cycles of activation in 0.1 M H_2SO_4. B) CV scans in 1 M H_2SO_4 of flat and nanoporous AIROFs. C) CV scans in phosphate buffered saline of flat and nanoporous AIROFs demonstrating the enhancement in CSC_c.

The AIROFs are also characterized by CV in 1 M H_2SO_4. As shown in **Figure 9B**, both flat and nanoporous AIROFs exhibit peaks at 0.34 and 0.155 V due to faradaic reactions between the Ir^{3+} and Ir^{4+} redox states within the IrOx film, thus confirming the formation of IrOx during activation. The enhanced currents exhibited by the nanoporous AIROFs are due to the increased infiltration of the nanoporous template and increased volume of IrOx formed during activation.

Additionally, as shown in **Figure 9C**, the nanoporous AIROFs exhibit enhanced CSC_c, with the 5 and 10 sec $Ir(acac)_3$ nanoporous AIROFs exhibiting 127 and 311 mC/cm^2, respectively, and the flat AIROF exhibiting 18.7 mC/cm^2. The large CSC_c of nanoporous AIROFs is highly desirable, as more charge can be delivered per stimulation pulse. However, the magnitude of the CSC_c is also significant with regards to mechanical stability. With more conventional AIROFs formed on Ir thin films or foils, large CSC_c values are commonly achieved by forming thicker IrOx films. However, these thicker IrOx film are more likely to exhibit delamination or other mechanical failures, especially at $CSC_c > 80$ mC/cm^2. However, the nanoporous AIROFs are less susceptible to these problems, as the primary factor determining CSC_c is the infiltration depth of the Ir ALD film rather than the thickness of the IrOx film. As a result, the nanoporous morphology enables a large CSC_c to be achieved with relatively thin IrOx films that do not suffer from delamination. This mechanical robustness was confirmed by the nanoporous AIROFs exhibiting no reduction in CSC_c after being subjected to ultrasonication treatments. The ability to achieve large CSC_c with thin IrOx films also has significant practical advantages, in that fewer activation cycles are required, which allows for quicker fabrication of such films.

Both flat and nanoporous AIROFs exhibit similar pH responses, with the flat AIROF exhibiting a slope of 69.2 mV/pH and the nanoporous AIROF exhibiting 67.5 mV/pH. The similar pH responses demonstrate that the nanoporous morphology does not significantly affect the film characteristics. Furthermore, the slope of the pH response provides information regarding the hydration of the IrOx film. As anhydrous IrO_2 is characterized by a Nernstian response with a slope of ~59 mV/pH, the super-Nernstian response indicates that the AIROFs are at least partially hydrous in nature, which is consistent with AIROF synthesis.

The application of ALD to AAO templates allows for the synthesis of nanoporous Ir films and AIROFs, and provides a number of advantages over alternative synthesis strategies. ALD enables precise control over the Ir film thickness and infiltration depth, while AAO provides a well-defined, tunable nanoporous template. The precise control over film morphology is especially important considering the significant volume expansion observed upon IrOx formation. By utilizing appropriate ALD templates, AIROFs retaining a highly nanoporous morphology can be synthesized. This nanoporous morphology yields significantly enhanced CSC_c values of 311 mC/cm^2 for nanoporous AIROFs compared to only 18.7 mC/cm^2 for flat AIROFs, while also maintaining the mechanical stability of thinner IrOx films. Additionally, both flat and nanoporous AIROFs exhibit similar pH responses, which demonstrate the potential for these films in pH sensing applications. Lastly, due to the precise control and tunability of the nanoporous AIROF film morphology enabled by AAO templates and ALD, future work will focus on investigating the effects of AIROF porosity in neural stimulation applications and on determining optimal porosities and film structures for such applications.

4. Development and Demonstration of SECM-SICM Imaging

In recent years, scanning ion conductance microscopy (SICM) has emerged as a versatile "non-contact" imaging tool. As such, SICM has been applied to numerous biophysical systems, including proteins in cell membranes, suspended artificial membranes, ionic conductivity of porous membranes, and mechanical properties of living cells. In addition, SICM has been further developed by integrating complementary techniques, including confocal microscopy, scanning near field optical microscopy (SNOM), and patch clamping. These auxiliary measurements provide additional information about the sample that is correlated with the surface topography detected by SICM imaging. Despite these impressive advancements in SICM, it remains insensitive to electrochemical properties. Spatial mapping of electrochemistry is commonly achieved by scanning electrochemical imaging (SECM) and has been widely used in the study of electrode surfaces, membrane transport, and biological systems. Over the past year, we have advanced the capabilities of SICM for electrochemical imaging by developing and demonstrating a nanopipette probe with an integrated ultramicroelectrode (UME) for concurrent SICM and SECM imaging.

The SECM-SICM probe fabrication procedure is shown in **Figure 10**. Nanopipettes were pulled from borosilicate glass capillaries (1 mm outer diameter, 0.5 mm inner diameter with filament, Sutter Instruments, Novato, CA) with a CO_2 laser-based pipette puller (P-2000, Sutter Instruments). Through experimentation with puller recipes, the pipette tips were consistently 200 nm in diameter with a 100 nm diameter opening, as measured by scanning electron microscopy (SEM). A 200-250 nm gold electrode film with a 5 nm titanium adhesion layer was electron beam evaporated onto one side of the pipette. The gold-coated pipette was then insulated by 70-100 nm of Al_2O_3 deposited by atomic layer deposition (ALD) in a viscous flow

type reactor. Al_2O_3 films were deposited at a temperature of 200°C with trimethylaluminum and H_2O reactants iteratively pulsed into the reactors at dose times of 1 second and purge times of 5 seconds. The Al_2O_3 deposition rate was approximately 0.105 nm/cycle. Lastly, the pipettes were focused ion beam (FIB) milled to expose the gold film as a UME and ensure an open pipette tip. FIB milling was conducted in a dual-beam FIB (FEI Helios, Hillsboro, OR) with a 30 kV, 0.28 pA ion beam. Pipettes were mounted gold side down onto the stage with conductive copper tape to ensure electrical contact to the pipette and minimize charging during image and milling. Milling was conducted normal to pipette axis in a multi-step process. The pipette was first milled to an outer diameter of approximately 800 nm. SEM imaging was then used to confirm that the UME was exposed and that the pipette tip was open. After confirmation, a final single pass milling step was used to clean the exposed microelectrode surface.

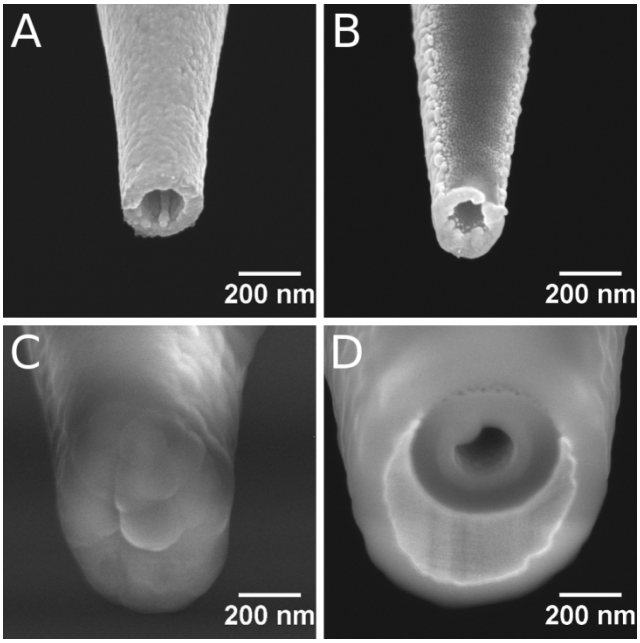

Figure 10. Scanning electron microscopy images of the SECM-SICM nanopipette at different points in the fabrication process. (A) After pipette pulling with 30 nm AuPd film to minimize charging. (B) After evaporation of the Ti/Au electrode film. (C) After atomic layer deposition of a 100 nm thick Al_2O_3 film. (D) After focused ion beam milling to open the nanopipette and expose the Au ultramicroelectrode.

A schematic of the SECM-SICM instrumentation is shown in **Figure 11**. SICM imaging was achieved with a commercially available SICM instrument (ScanIC, ionscope, London, U.K.). The pipette was mounted onto a single-axis piezo scanner for pipette oscillation and feedback-controlled movement of the pipette in the z direction. Samples were placed into a small petri dish filled with solution. The petri dish rests on a separate piezo scanner that rasters in the x and y directions for SICM imaging. The entire SICM microscope rests above an inverted optical microscope stage for positioning of the pipette relative to the sample.

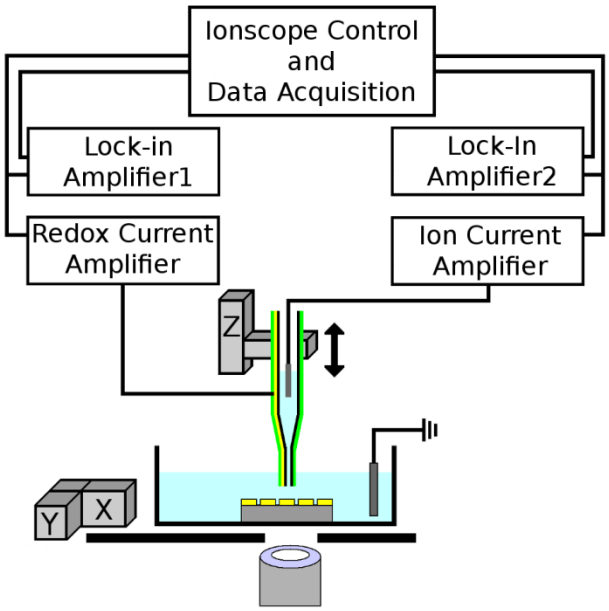

Figure 11. Schematic of the SECM-SICM imaging instrumentation.

Conventional SICM imaging utilizes two electrodes. A Ag/AgCl electrode in the bath solution was grounded and served as the reference electrode for all applied voltages, and a separate Ag/AgCl electrode was placed inside of the pipette and biased to generate an ion current through the pipette tip. This ion current was amplified, with the AC component of the ion current detected by the SICM hardware and serving as the feedback signal for topographic imaging. For integrated SECM-SICM imaging, a third electrode connection was made to the UME. Voltages were applied and the redox current was amplified by a low-noise patch-clamp amplifier (AxoPatch 200B, Molecular Devices, Sunnyvale, CA). The AC components of both the ion and redox currents at the pipette oscillation frequency were measured using two separate lock-in amplifiers (SR850, Stanford Research Systems, Sunnyvale, CA). A low-noise digitizer (Digidata 1440A, Molecular Devices) was used to apply all electrode biases and to monitor and record all signals.

Integrated SECM-SICM imaging has been demonstrated feedback mode imaging on patterned substrates. Feedback mode imaging was conducted on FIB-milled substrates in a solution of 10 mM $Ru(NH_3)_6Cl_3$, 100 mM KNO_3. **Figure 12** shows SEM images of the fabricated test structures and corresponding SECM-SICM topography, DC redox current, and AC redox current images. The substrates consist of 400 nm wide trenches with a center-to-center spacing of 2.6 μm that were FIB-milled into a gold film to expose the underlying glass substrate. These recessed features are narrower than the overall diameter of the fabricated SECM-SICM probe, preventing the full extension of the probe into the trench; yet the trenches are still detected in the SICM topography image, indicating successful surface tracking via SICM feedback and allowing comparison between the topographic and electrochemical features.

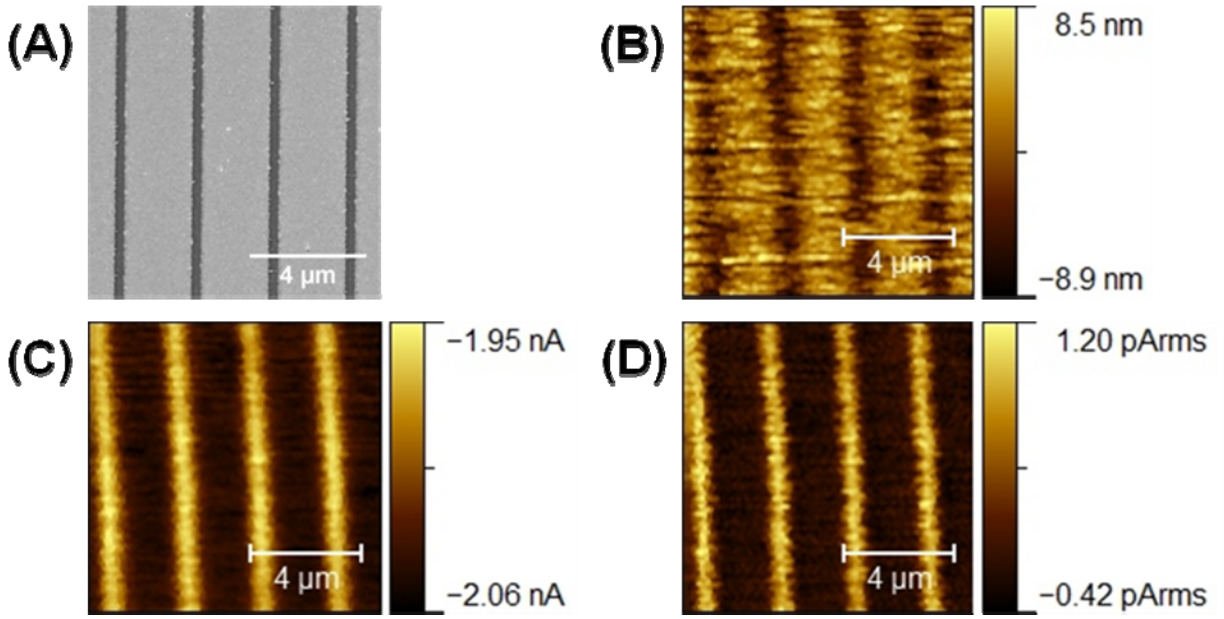

Figure 12. SEM and feedback-mode SECM-SICM images of 400 nm wide trenches that were FIB-milled into a gold film to expose the underlying glass substrate. The images were taken in 10 mM $Ru(NH_3)_6^{3+}$, 100 mM KNO_3. (A) SEM, (B) SECM-SICM topography, (C) SECM-SICM DC redox current, (D) SECM-SICM AC redox current.

Correlation of the topography and redox current images reveals the expected contrast in both the DC and AC redox current images, with enhanced current over the broad Au regions, consistent with positive feedback, and reduced current over the narrow insulating trenches, consistent with negative feedback. As shown in the line profile in **Figure 13**, the redox current signals exhibit some convolution between the trench and UME dimensions, resulting in an observed full width at half maximum (FWHM) of 680 nm in the DC redox current and 580 nm in the AC redox current. Despite this broadening, the UME is capable of resolving the trenches as isolated features, with the redox current returning to a constant value between the trenches. The line profile also reveals a lateral offset between the topographic and redox current signals of approximately 230 nm, which is consistent with the center-to-center separation of the nanopipette tip opening and the integrated UME.

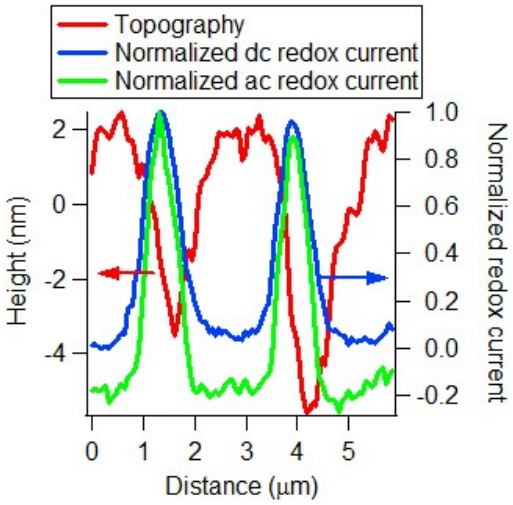

Figure 13. Line profile of the SECM-SICM topography, DC redox current and AC redox current on the 400 nm wide FIB-milled patterns from Figure 12.

As shown in **Figure 14**, SECM-SICM images were also acquired of 180 nm wide trenches separated by 875 nm to further characterize the spatial resolution of the probes. At these reduced dimensions, the probes are still capable of detecting the trenches in SICM topography, DC redox current, and AC redox current images. Despite the increased significance of the lateral broadening relative to the inter-trench spacing, the probes are still capable of resolving individual trenches. Based on these images, it is clear that the probes are capable of detecting features in the deep sub-micron regime.

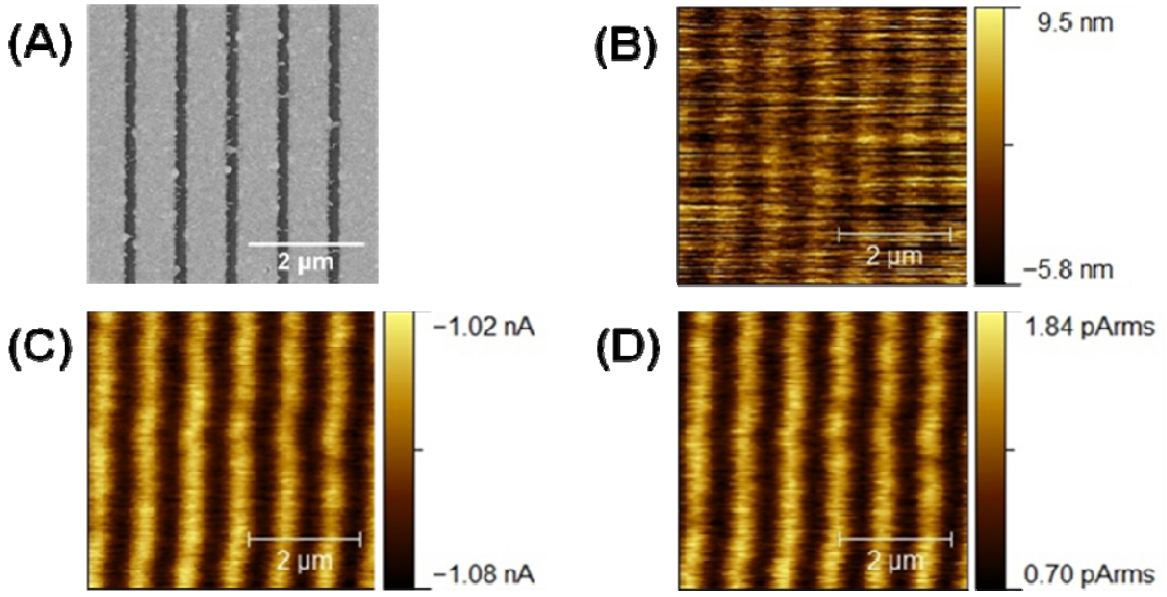

Figure 14. SEM and feedback-mode SECM-SICM images of 180 nm wide trenches that were FIB-milled into a gold film to expose the underlying glass substrate. The images were taken in 10 mM $Ru(NH_3)_6^{3+}$, 100 mM KNO_3. (A) SEM, (B) SECM-SICM topography, (C) SECM-SICM DC redox current, (D) SECM-SICM AC redox current.

5. Fabricating and Characterizing Nanoporous AAO Membranes

Anodized aluminum oxide (AAO) is an ideal prototype substrate for studying ion transport through nanoporous membranes. For optimal performance, it is highly desirable to independently control the width, height, and spacing of the pores in AAO. AAO templates are typically fabricated through a two-step anodization process. In the first step, a disordered nanoporous alumina film is created following constant voltage anodization of aluminum. As the film grows, the pores self-order over a period of hours, leading to a hexagonally ordered arrangement at the sub-surface growth front. When this initial alumina film is removed, the resulting aluminum surface possesses a hexagonally ordered arrangement of pits. These pits serve as pore nucleation sites during the second anodization step, thus yielding a highly uniform and ordered nanoporous AAO film. This two-step procedure creates ordered nanoporous arrays in sulfuric, oxalic, malonic, and phosphoric acids at 25 V, 40 V, 130 V, and 195 V with inter-pore spacings of 63 nm, 100 nm, 250 nm, and 500 nm respectively. By modifying the anodization solution and using higher than self-ordering voltages, additional inter-pore spacings have been achieved, but these conditions are not well-suited to thin film anodization. Consequently, aluminum pretexturing is required to form ordered AAO with arbitrary inter-pore spacings.

A number of patterning techniques have been explored to create ordered pits in aluminum as a precursor to AAO. For example, imprinting techniques using a mold fabricated by interference lithography, self-assembly of nanoparticles, or anodization have been shown to be effective. However, these techniques utilize large pressures rendering them unsuitable for aluminum thin films on brittle substrates, such as glass or silicon. Alternatively, aluminum can be evaporated onto hexagonally ordered nanospheres and then cleaved from the substrate to create ordered pits. Other strategies have employed reactive ion etching (RIE) with masks of through-hole AAO and diblock copolymers to create a textured aluminum surface. While each of these techniques possesses distinct advantages compared to the traditional two-step anodization process, their limited process latitude presents challenges for the fabrication of nanoporous membranes with arbitrarily tunable inter-pore spacing, pore diameter, and aspect ratio.

On the other hand, nanosphere lithography (NSL) is a technique that has been widely utilized to create periodic nanostructures due to its simple processing and controllable periodicity. In NSL, nanospheres of polystyrene (PS) or other materials are self-assembled onto a substrate into a hexagonally close-packed monolayer. Nanospheres can be deposited by a variety of methods including spin coating, dip coating, and evaporation to create this ordered monolayer. By controlling the nanosphere diameter and surface chemistry, the monolayer periodicity and ordering can be widely tuned.

Over the past year, we have employed NSL to pre-texture aluminum films on a variety of substrates to create AAO films with tunable inter-pore spacing, pore diameter, and aspect ratio. First, an aluminum thin film of the desired thickness is deposited on a selected substrate by thermal evaporation (**Figure 15A**). The Al surface is then pretreated by spinning a solution of Triton-X 100 surfactant and water to increase its hydrophilicity, which has been shown to be important in nanosphere ordering. A nanosphere solution containing water, PS spheres, and Triton-X 100 for sphere diameters of 80 nm and 160 nm, or water, methanol, PS spheres, and Triton-X 100 for 240 nm diameter spheres is then spun onto the Al surface. This procedure results in a hexagonally close-packed monolayer of PS spheres (**Figure 15B**). The monolayer is

subsequently etched using RIE with a 3:2 mixture of Ar:O_2 to reduce the nanosphere diameter. At this point, tungsten is sputter deposited, and the spheres are removed by sonicating in toluene at 70ºC (**Figures 15C-E**), leaving a tungsten film with an ordered array of holes. The tungsten is then used as a mask for nitric and phosphoric acid etching of the aluminum to create ordered pits in the Al surface, which serve as templates for AAO. In particular, the textured Al surface is anodized in 0ºC phosphoric acid at 50 V, 100 V, and 150 V for sphere diameters of 80 nm, 160 nm, and 240 nm respectively. Finally, the tungsten is selectively removed in an aqueous solution of potassium ferricyanide (**Figure 15F**). This process has been successfully performed on glass, silicon, and silicon nitride surfaces.

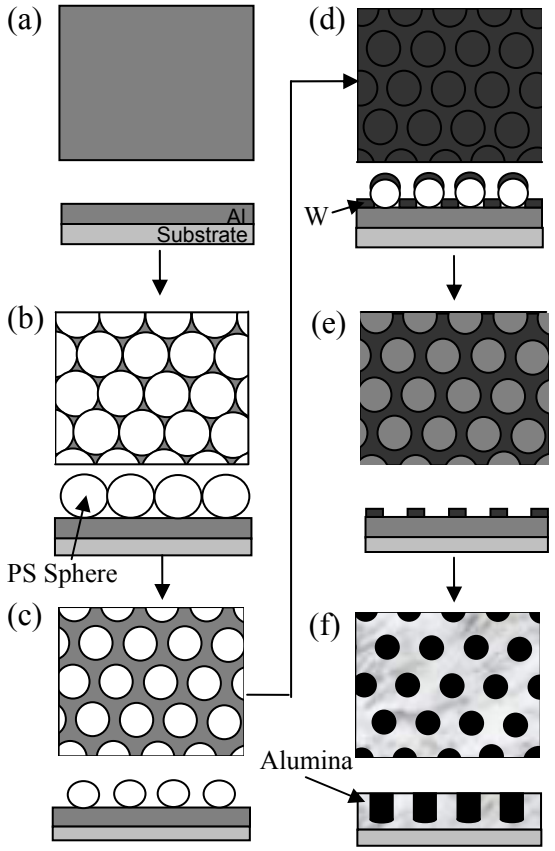

Figure 15. Schematic diagrams (top view and cross-sectional view) of the NSL-based anodization procedure: (a) Aluminum coated substrate; (b) Monolayer of assembled polystyrene nanospheres; (c) Etched polystyrene nanospheres; (d) Deposited tungsten film; (e) Nanospheres removed to yield openings in the tungsten film; (f) Final anodized alumina film.

Scanning electron microscopy (SEM) micrographs of the completed structures in **Figure 16** show the uniformity of the pore size and inter-pore spacing. The inter-pore spacing is measured to be 84 nm, 154 nm, and 234 nm with pore diameters of 33 nm, 57 nm, and 70 nm for 80 nm, 160 nm, and 240 nm diameter spheres respectively. The inter-pore spacings closely match the nominal initial sphere diameters as expected. The 80 nm diameter spheres exhibit reduced ordering compared to the larger sphere sizes since they possess higher polydispersity. The pore diameter can be widened controllably using 5% phosphoric acid to create any larger pore size. Furthermore, the pore aspect ratio can be controlled by varying the deposited Al

thickness as shown in **Figure 17**. The AAO thicknesses are 400 nm, 700 nm, and 1000 nm for a deposited Al thickness of 300 nm, 400 nm, and 500 nm respectively when using 240 nm diameter spheres. It should also be noted that the pores are straight and do not split.

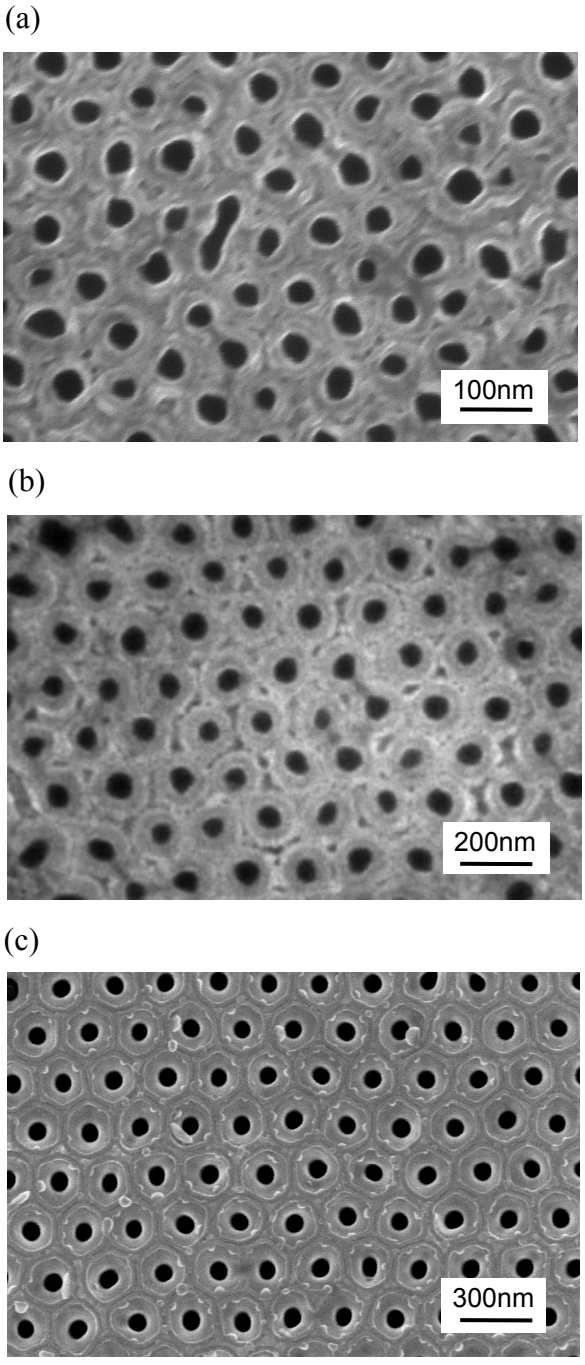

Figure 16. Scanning electron microscope images of the final AAO nanopore structures fabricated using (a) 80 nm, (b) 160nm, and (c) 240 nm nanosphere diameters.

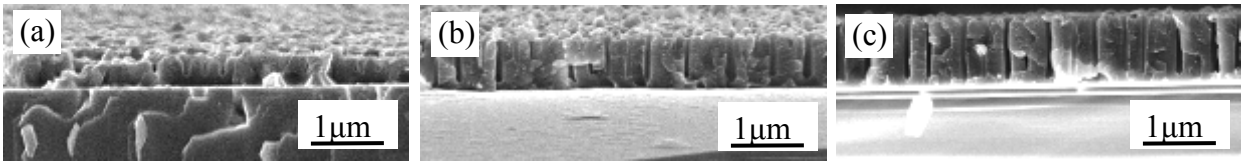

Figure 17. SEM cross-sectional images of the final AAO nanopore structures fabricated using 240 nm diameter nanospheres and (a) 300 nm, (b) 400 nm, and (c) 500 nm thick aluminum films.

Supported nanoporous membranes are fabricated using a process similar to that of Si_3N_4 membrane fabrication. A Si(100) substrate is first coated with low pressure chemical vapor deposition Si_3N_4 (**Figure 18A**). Subsequently, photolithography and RIE with CF_4 and O_2 are used to etch apertures in the back (unpolished) Si_3N_4 layer. Aluminum is then deposited on the front (polished) side of the substrate and the NSL procedure is used to create AAO (**Figure 18B**). The sample is then sealed into a Teflon holder with Viton gaskets such that only the back (unpolished) side is exposed. Substrate etching is achieved in KOH, which is an anisotropic etch for the {100} planes over the {111} planes. The etching is carried out until the etch stops at the top Si_3N_4 layer, which is detected by the appearance of optical transparency. RIE with CF_4 and O_2 removes the Si_3N_4, and finally the AAO barrier oxide layer is removed in 5% phosphoric acid (**Figure 18C**).

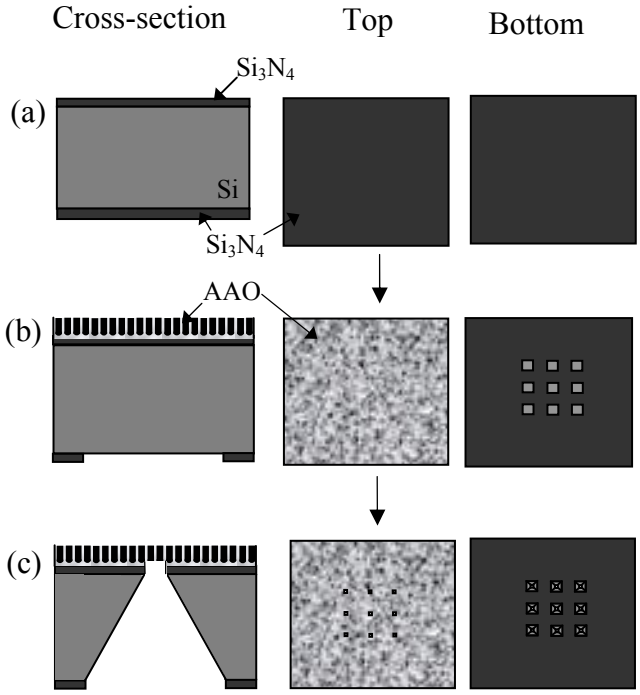

Figure 18. Schematic diagrams of the processing steps used to achieve nanoporous AAO membranes. The left column is the cross-sectional view, the middle column is the polished side of the wafer, and the right column is the unpolished side of the wafer. (a) Initial silicon nitride coated silicon substrate. (b) AAO is formed on the top surface using the NSL-based anodization procedure, and an opening is patterned in the silicon nitride on the back surface. (c) Final nanoporous structure following etching of the silicon substrate, silicon nitride film, and AAO oxide barrier layer.

A transmitted electron image of a nanoporous membrane created with 240 nm diameter spheres and a 400 nm thick deposited Al film is shown in **Figure 19**. The bright spots indicate through-hole pores in the image since the transmission of electrons is unimpeded. The through-hole pores are observed with a high coverage over the entire membrane. Furthermore, the low voltage secondary electron and transmitted electron images in **Figures 19B-C** do not detect any contrast over the pores. Due to the high surface sensitivity and low penetration depth of low energy electrons, these low voltage images confirm that the pores are indeed through-hole. To further show through-hole nanoporous behavior, ionic conductance measurements were performed before and after etching the AAO barrier layer. Prior to etching, the ionic conductance is less than 1 nS in aqueous 1 M KCl. On the other hand, after removal of the barrier layer, the ionic conductance increases by three orders of magnitude, revealing the through-hole nature of the pores. In particular, **Figure 20** reveals that the ionic conductance plateaus for increasing values of the KCl concentration. Similar ionic conductance plateau behavior has been found both theoretically and experimentally for through-hole nanopores in polymer membranes.

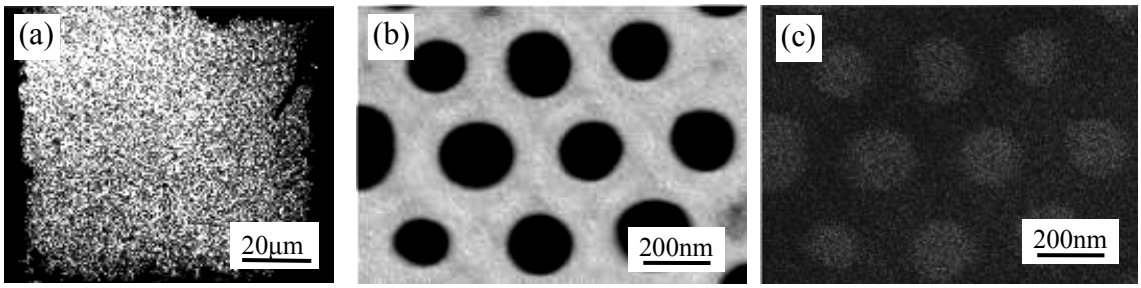

Figure 19. Scanning electron microscopy images of the completed nanoporous membranes viewed from the unpolished side of the wafer. (a) Transmitted electron image with 30 kV accelerating voltage of the entire membrane. (b) Image taken at 1 kV accelerating voltage using the secondary electron detector. (c) The same image as in part b except using the transmitted electron detector.

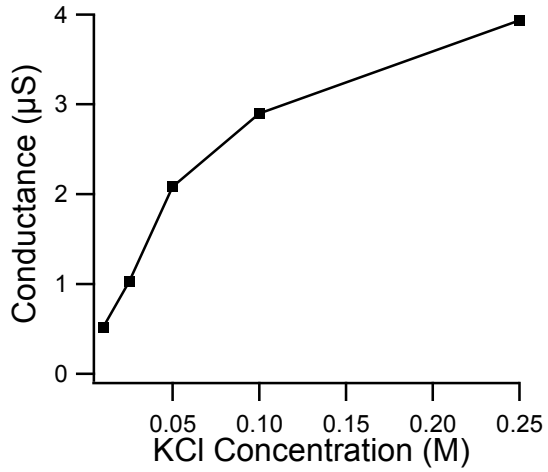

Figure 20. Ionic conductance through an AAO nanoporous membrane as a function of KCl concentration.